Spectrin regulates cell contractility through production and maintenance of actin bundles in the *Caenorhabditis elegans* spermatheca

Alison C. E. Wirshing and Erin J. Cram*
Department of Biology, Northeastern University, Boston, MA 02115

ABSTRACT **Disruption to the contractility of cells, including smooth muscle cells of the cardiovascular system and myoepithelial cells of the glandular epithelium, contributes to the pathophysiology of contractile tissue diseases, including asthma, hypertension, and primary Sjögren's syndrome. Cell contractility is determined by myosin activity and actomyosin network organization and is mediated by hundreds of protein–protein interactions, many directly involving actin. Here we use a candidate RNA interference screen of more than 100 *Caenorhabditis elegans* genes with predicted actin-binding and regulatory domains to identify genes that contribute to the contractility of the somatic gonad. We identify the spectrin cytoskeleton composed of SPC-1/α-spectrin, UNC-70/β-spectrin, and SMA-1/β heavy-spectrin as required for contractility and actin organization in the myoepithelial cells of the *C. elegans* spermatheca. We use imaging of fixed and live animals as well as tissue- and developmental-stage-specific disruption of the spectrin cytoskeleton to show that spectrin regulates the production of prominent central actin bundles and is required for maintenance of central actin bundles throughout successive rounds of stretch and contraction. We conclude that the spectrin cytoskeleton contributes to spermathecal contractility by promoting maintenance of the robust actomyosin bundles that drive contraction.**

Monitoring Editor
Jeffrey D. Hardin
University of Wisconsin

Received: Jun 7, 2018
Revised: Jul 23, 2018
Accepted: Jul 27, 2018

INTRODUCTION

Actin and the actin motor protein myosin form contractile actomyosin networks involved in the perception and production of forces in contractile nonmuscle cells (Burridge and Wittchen, 2013; Zaidel-Bar *et al.*, 2015; Svitkina, 2018). These include smooth muscle cells of the cardiovascular and gastrointestinal systems as well as myoepithelial cells of the glandular epithelium. Disruption to actomyosin network organization and myosin activity contributes to the pathophysiology of contractile tissue diseases, including asthma (Ammit *et al.*, 2000; Flores *et al.*, 2007; Gao *et al.*, 2007; Lavoie *et al.*, 2009; Leguillette *et al.*, 2009), hypertension (Uehata *et al.*, 1997), and primary Sjögren's syndrome, a disease affecting the lacrimal and salivary glands resulting in dry mouth and eyes (Sisto *et al.*, 2018). Understanding the mechanisms that regulate actomyosin networks is complicated by the fact that actin is involved in more protein–protein interactions than any other protein (Dominguez, 2004) and has more than 100 different binding partners (Dos Remedios *et al.*, 2003). Contraction in nonmuscle cells alone is regulated by 230 specific interactions and counting (Zaidel-Bar *et al.*, 2015). To identify actin-binding and regulatory proteins involved in actomyosin network organization and tissue contractility in vivo, we used a candidate RNA interference (RNAi) screen approach to identify actin-binding and regulatory genes required for contractility of the myoepithelial cells of the *Caenorhabditis elegans* spermatheca.

The spermatheca is an organ of the *C. elegans* somatic gonad composed of a monolayer of 24 myoepithelial cells that surround and contain the sperm (Hirsh *et al.*, 1976; Hubbard and Greenstein, 2000). *Caenorhabditis elegans* is hermaphroditic, producing both eggs and sperm in two symmetrical gonad arms that connect

This article was published online ahead of print in MBoC in Press (http://www.molbiolcell.org/cgi/doi/10.1091/mbc.E18-06-0347) on August 9, 2018.

*Address correspondence to: Erin J. Cram (e.cram@neu.edu).

Abbreviations used: AID, auxin-inducible decay; F-actin, filamentous-actin; G-actin, globular-actin; GFP, green fluorescent protein; MLCK, myosin light-chain kinase; RNAi, RNA interference; SP-UT, spermathecal–uterine.

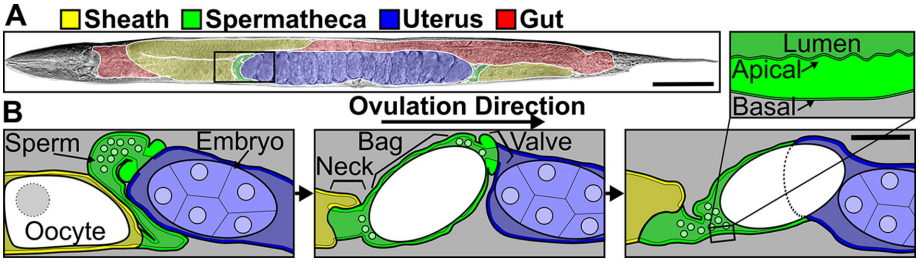

FIGURE 1: Diagram of the *C. elegans* somatic gonad. (A) Brightfield image of an adult hermaphrodite false colored to indicate the sheath cells (yellow), spermathecae (green), uterus (blue), and gut (red). (B) Diagram of the area indicated by a black box in A during an ovulation. First panel: sheath cell contractions begin to push the proximal oocyte (white). Second panel: sheath contractions force the oocyte into the spermatheca, where it is fertilized. Third panel: the spermathecal-uterine valve opens as the spermathecal bag contracts to expel the fertilized embryo into the uterus. Insert in B shows a magnified cross-section of the spermatheca indicating that the apical surface faces the lumen. Scale bars, 50 μm in A and 20 μm in B.

to a common uterus (Figure 1). Each gonad arm contains contractile sheath cells and the spermatheca. During ovulation, sheath cells surrounding the developing oocytes contract to push the proximal oocyte into the spermatheca; the spermatheca is stretched by the incoming oocyte, the oocyte resides in the spermatheca while fertilization occurs and the eggshell develops, and then coordinated spermathecal cell contractions expel the embryo through the spermathecal–uterine (SP-UT) valve and into the uterus (Figure 1) (Hirsh *et al.*, 1976; Ward and Carrel, 1979; Hubbard and Greenstein, 2000). This process occurs ~150 times per gonad arm, requiring robust regulation of spermathecal contractility. We and others have shown that the actin cytoskeleton plays a central role in spermathecal contractility (Deng *et al.*, 2007; Kovacevic and Cram, 2010; Hegsted *et al.*, 2016; Wirshing and Cram, 2017). The most prominent spermathecal actin cytoskeletal features are stress-fiber-like actomyosin bundles that are oriented along the long axis of each cell (Wirshing and Cram, 2017). These bundles develop concomitantly with contraction during the first ovulation and are maintained throughout adulthood (Wirshing and Cram, 2017). Myosin activity is required for bundle development (Wirshing and Cram, 2017; Kelley *et al.*, 2018). However, myosin is clearly not the only actin interacting protein involved in regulating spermathecal actin organization (Deng *et al.*, 2007; Kovacevic and Cram, 2010; Hegsted *et al.*, 2016) and the molecular mechanisms allowing for bundle maintenance during successive rounds of ovulation are largely unknown.

In our candidate RNAi screen of 102 genes with predicted actin-binding and regulatory domains we identified *unc-70* and *sma-1*, encoding the *C. elegans* β- and β heavy-spectrin, respectively, as required for spermathecal contractility. Spectrin was first discovered in erythrocytes (Yu *et al.*, 1973) where it functions to provide mechanical durability to the erythrocyte membrane (Greenquist *et al.*, 1978; Tse *et al.*, 1990). Since its discovery in erythrocytes, it has been shown that nonerythroid isoforms of spectrin are broadly expressed in different cell types and have diverse functions (Bennett and Baines, 2001; Zhang *et al.*, 2013; Machnicka *et al.*, 2014). In addition to providing mechanical durability, the spectrin cytoskeleton is involved in vesicle transport (Holleran *et al.*, 1996; Devarajan *et al.*, 1997; Stankewich *et al.*, 1998; Holleran et al., 2001; Muresan *et al.*, 2001; Johansson *et al.*, 2007), establishment or maintenance of cell polarity (Nelson *et al.*, 1990; Dubreuil *et al.*, 1997, 2000; Piepenhagen and Nelson, 1998), and regulation of the actomyosin cytoskeleton (Benz *et al.*, 2008; Metral *et al.*, 2009; Ponceau *et al.*, 2015; Wong *et al.*, 2015). Spectrin forms heterodimers composed of one α and one β subunit aligned in an anti-parallel orientation. Through head-to-head interactions, these dimers form tetramers that are capable of binding and cross-linking short actin filaments to form the spectrin-actin cytoskeleton (Li *et al.*, 2008, 2010). Spectrin heterotetramers form a meshwork at the cell plasma membrane and have also been observed associated with organelles including the Golgi (Devarajan *et al.*, 1997; Stankewich *et al.*, 1998) endoplasmic reticulum (ER) (Lencesova *et al.*, 2004), and nucleus (McMahon *et al.*, 1999).

In vertebrates, there are two α- and five β-spectrins. The αI and βI isoforms are erythrocyte specific, while αII and βII are broadly expressed (Moon and McMahon, 1990; Cianci *et al.*, 1999). *Caenorhabditis elegans* has one α-, SPC-1/α, and two β-spectrins, a conventional β-spectrin, UNC-70/β, and a β heavy-spectrin, SMA-1/βH. β heavy-spectrin has additional spectrin repeats, an SRC homology 3 domain (SH3) protein–protein interaction domain, and unique binding partners and functions (Médina *et al.*, 2002; Lee *et al.*, 2010b). UNC-70/β and SMA-1/βH have distinct expression patterns and subcellular localizations with the expression and function of SMA-1/βH restricted to a specific subset of tissues (McKeown *et al.*, 1998; Buechner *et al.*, 1999; Norman and Moerman, 2002; Ferrier *et al.*, 2011). However, mutations in SMA-1/βH enhance the UNC-70/β loss of function phenotype, indicating that the two β isoforms have some overlapping functions (Norman and Moerman, 2002). In *C. elegans*, spectrin is required for cell shape changes during embryonic morphogenesis (McKeown *et al.*, 1998; Moorthy *et al.*, 2000; Norman and Moerman, 2002; Praitis *et al.*, 2005), actin organization within the body wall muscles and hypodermis (Hammarlund *et al.*, 2000; Moorthy *et al.*, 2000; Norman and Moerman, 2002; Praitis *et al.*, 2005), and the mechanical durability of neurons (Hammarlund *et al.*, 2007, Krieg *et al.*, 2014). While spectrin has been shown to contribute to *C. elegans* reproduction through regulating egg-laying and embryogenesis (McKeown *et al.*, 1998; Moorthy *et al.*, 2000; Norman and Moerman, 2002; Praitis *et al.*, 2005), the role of spectrin in the spermatheca was unknown. Here we show that SPC-1/α, UNC-70/β, and SMA-1/βH are expressed in the spermatheca and the SP-UT valve. We find that loss of the spectrin reduces spermathecal contractility and alters actomyosin network organization. We use auxin inducible decay (AID) to deplete spectrin postdevelopment and show a role for spectrin beyond morphogenesis. Additionally, we use time-lapse confocal microscopy of live animals to show that alterations to the spectrin cytoskeleton influence actin dynamics. This work contributes to our understanding of the diverse roles of the spectrin cytoskeleton and demonstrates a role for spectrin outside of morphogenesis or the nervous system in *C. elegans*. We provide evidence that spectrin influences spermathecal contractility through regulating the organization and dynamics of the stress-fiber-like actomyosin bundles.

RESULTS

A screen of genes for actin-binding and regulatory proteins in *C. elegans* reveals that spectrin is involved in spermathecal contractility

To identify actin-binding and regulatory proteins required for spermathecal contractility and actin organization, we used a candidate RNAi screen approach. The Ontology Browser on WormBase

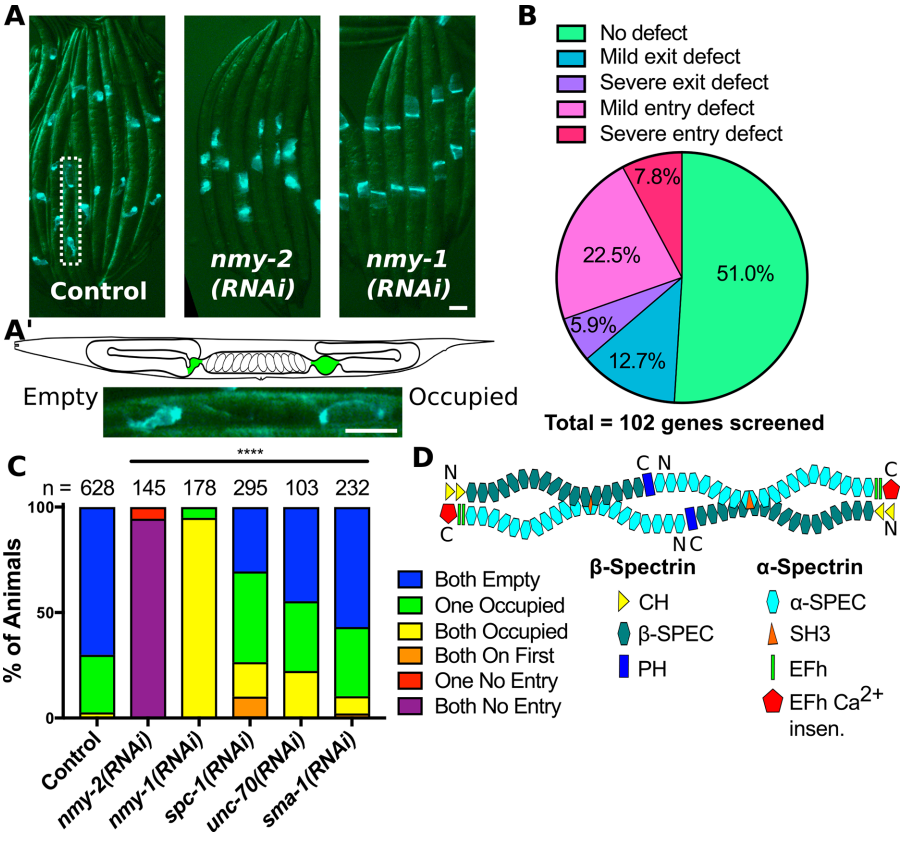

FIGURE 2: A screen of *C. elegans* genes encoding actin-binding proteins reveals spectrin is required for spermathecal contractility. (A) Images of whole animals expressing GFP::ACT-1 in the spermatheca treated with control RNAi, and RNAi against *nmy-2* and *nmy-1*. Note the lack of embryos in the uteri of *nmy-2(RNAi)* animals and the increase in occupied spermathecae in *nmy-1(RNAi)* animals. (A′) A schematic of the *C. elegans* reproductive system with the spermathecae highlighted in green above a magnified insert of the area indicated by a dotted line in A, showing one occupied and one empty spermatheca in the same animal. (B) A summary of the somatic gonad contractility phenotypes observed for the 102 genes encoding actin-binding proteins screened. Genes that disrupt the sheath result in entry defects. For an example, see *nmy-2(RNAi)* in C. Genes that disrupt the spermatheca result in exit defects. For an example, see *nmy-1(RNAi)* in C. (C) Scoring results for animals treated with the indicated RNAi. Spermathecae undergoing ovulation that are occupied by an oocyte and appear distended are scored as occupied, and spermathecae between ovulations that contain only sperm and appear compact are scored as empty. Animals with occupied spermathecae but no embryos in the uterus are scored as "occupied on first," and animals with empty spermathecae and no embryos in the uterus are scored as "no entry." (D) Schematic of a spectrin heterotetramer composed of α-spectrin and β-spectrin subunits. UNC-70/β has two tandem, N-terminal, actin-binding, calponin homology domains (CH), 17 spectrin repeats (β-SPEC), and a C-terminal pleckstrin homology domain (PH). SPC-1/α has 20 spectrin repeats (α-SPEC), an SH3 within the ninth spectrin repeat, two tandem Ca^{2+}-binding EF-hand domains (EFh), and a C-terminal Ca^{2+}-insensitive domain (EFh Ca^{2+} insen.). Scale bars, 50 μm and 20 in the insert. Chi-square test, *p* value: ****$p \leq 0.0001$, *n* = number of animals scored.

(wormbase.org) was used to identify genes that encode proteins with conserved domains for actin-binding and actin filament organization. In total, 102 genes were screened for spermathecal contractility defects in a line expressing actin labeled with green fluorescent protein (GFP) in the spermatheca (Supplemental Figure 1 and Supplemental Table 1). The GFP allows for easy visualization of the spermatheca under the dissection scope. With this line, we can distinguish spermathecae undergoing ovulation that are occupied by an oocyte and appear distended, termed "occupied," from spermathecae between ovulations that contain only sperm and appear compact, termed "empty" (Figure 2A). In wild-type (WT) animals, ovulation occurs over ~10 min, and the spermatheca spends most of the time unoccupied between ovulations (Ward and Carrel, 1979). Consistent with this, we find that 71.7 ± 7.9% of animals fed control RNAi have two empty spermathecae, 25.4 ± 7.0% have one occupied and one empty spermatheca, and only 2.8 ± 1.3% have two occupied spermathecae (mean ± SD, *n* = 1753 animals, 11 experiments). These percentages are highly reproducible between experiments, giving us confidence that deviation from this likely indicates a role for the RNAi candidate in spermathecal contractility (Supplemental Figure 2).

In addition to spermathecal contractions, sheath cell contractions and a functional germline that produces oocytes are also required for successful ovulation (Myers *et al.*, 1996; Ono and Ono, 2004, 2014, 2016; Ono *et al.*, 2007; Obinata *et al.*, 2010). Oocytes are produced from proliferative germ cells in the distal gonad that enter meiosis as they move proximally. The proliferative germ line and the transition to meiosis is regulated by soma-germ cell signaling (Mccarter *et al.*, 1997, 1999). These cells then mature into large oocytes in the proximal gonad through actin-dependent cytoplasmic streaming (Gibert *et al.*, 1984; Wolke *et al.*, 2007). At the start of ovulation, the most proximal oocyte is driven into the spermatheca by sheath cell contractions. Disruption of genes required for oogenesis results in an entry defect where no oocyte enters and expands the spermatheca (Cecchetelli *et al.*, 2016; Wirshing and Cram, 2017). Entry defects are also seen when disrupted sheath contractions prevents oocyte entry into the spermatheca, and the oocyte remains in the gonad arm (Myers *et al.*, 1996; Ono and Ono, 2004, 2014, 2016; Ono *et al.*, 2007; Obinata *et al.*, 2010). For example, the nonmuscle myosin II isoform, NMY-2, is part of the contractile machinery of the sheath (Ono and Ono, 2016) and also regulates germline morphology (Green *et al.*, 2011). RNAi of this gene produces an entry defect (Figure 2, A and C). This is distinct from the phenotype of animals with functional germlines and sheath cells but disrupted spermathecal contractions. In these animals, the oocyte enters but becomes trapped within the spermatheca as the spermatheca fails to contract and push the embryo into the uterus (Kovacevic and Cram, 2010; Kovacevic *et al.*, 2013; Wirshing and Cram, 2017; Kelley *et al.*, 2018). This is seen, for example, in animals depleted of the nonmuscle myosin II isoform, NMY-1 (Figure 2, A and C). In this way, we can partially distinguish genes primarily required for spermathecal contractility from genes involved in other aspects of the somatic gonad and germline. However, some proteins are common to multiple tissues within the reproductive system. For example, *lev-11*, tropomyosin, and *deb-1*, vinculin, are expressed in both the spermathecal and sheath cells (Ono *et al.*, 2007). Consistent with their roles in the sheath, RNAi of these

genes results in entry defects (Supplemental Figure 1 and Supplemental Table 1). However, we are unable to determine whether spermathecal contractility is also impacted. This suggests some of the genes we have identified as resulting in an entry defect may have functions in the spermatheca in addition to potential functions in other somatic and germline cells of the reproductive system.

Of the 102 genes screened, 49.0% result in ovulation defects highlighting the importance of the actin cytoskeleton in *C. elegans* reproduction. Of these genes, 30.4% result in entry defects (Figure 2B, Supplemental Figure 1, and Supplemental Table 1). Many of the genes resulting in severe entry defects have been described previously in the sheath: *tln-1* (Cram *et al.*, 2003), *nmy-2* (Ono and Ono, 2016), *unc-60* (Ono *et al.*, 2008), *unc-54*, *deb-1*, and *lev-11* (Ono *et al.*, 2007). Two, *ctn-1* and *nuo-3*, are potential novel regulators of *C. elegans* reproduction identified in our screen and may contribute to sheath development and contractility, germline development, or oogenesis (Supplemental Figure 1 and Supplemental Table 1). We also identified genes required for the spermathecal contractions that drive exit of the embryo from the spermatheca into the uterus including 6 (5.8%) genes that result in severe spermathecal exit defects (Figure 2B, Supplemental Figure 1, and Supplemental Table 1). Of these genes, we have previously characterized two, *nmy-1* and *fln-1*, encoding nonmuscle myosin II and filamin, respectively, as required for spermathecal contractility and actin organization (Kovacevic *et al.*, 2013; Wirshing and Cram, 2017). One, *unc-87*, encodes an actin-binding protein with some structural similarity to calponin but with no orthologues outside of nematodes (Kranewitter *et al.*, 2001). Another, *unc-115,* encodes a LIM domain containing protein homologous to abLIM involved in axon path finding (Lundquist *et al.*, 1998; Struckhoff and Lundquist, 2003; Yang and Lundquist, 2005; Shakir *et al.*, 2008; Demarco and Lundquist, 2010). The other two, *unc-70* and *sma-1*, encode β- and β-heavy spectrin, respectively, indicating spectrin is required for spermathecal contractility. Because two of our top hits impact the spectrin-actin cytoskeleton, we decided to characterize the role of spectrin in spermathecal contractility.

The spectrin-actin cytoskeleton is composed of heterotetramers formed from two α- and two β-spectrin subunits that bind through head-to-head interactions producing a rodlike spectrin tetramer with an actin-binding domain at each end (Li *et al.*, 2008, 2010). The interaction between α- and β-spectrin is required to form tetramers that are capable of cross-linking actin and producing the spectrin-actin cytoskeleton (Figure 2D). However, in *Drosophila* epithelial cells β-spectrin has α-spectrin independent functions (Dubreuil *et al.*, 2000). SPC-1/α was not initially included in our screen because it does not directly bind actin. To determine whether SPC-1/α is also required for spermathecal contractility, we scored animals as described above fed RNAi against *spc-1*. Depletion of SPC-1/α results in a more severe disruption to ovulation than depletion of either UNC-70/β or SMA-1/βH. We frequently observe animals with occupied spermathecae but no embryos in the uterus, indicating the oocyte is able to enter the spermatheca but not pass through the valve (Figure 2C). This is distinct from the phenotype observed with *nmy-1* depletion where the spermathecal bag and valve remain flaccid and sheath contractions continue to push oocytes through the distended spermathecal bag and valve (Kovacevic *et al.*, 2013). It may be that loss of SPC-1/α influences sheath function or the germline in addition to spermathecal contractility or disrupts the valve preventing embryo transit through the valve.

To confirm that the RNAi phenotypes observed are due to a specific loss of spectrin, we scored unlabeled WT, N2, and animals expressing the null allele of UNC-70/β, *unc-70(s1502)* (Johnsen and Baillie, 1991; Hammarlund *et al.*, 2007), as well as two alleles that result in single-amino-acid substitutions between spectrin repeats 16 and 17 of UNC-70/β, *unc70(e542)*, and *unc-70(n493)* (Krieg *et al.*, 2014). Spectrin repeats 16 and 17 of β-spectrin are involved in the interaction between β- and α-spectrin (Li *et al.*, 2008, 2010), and the two alleles are predicted to disrupt this interaction (Krieg *et al.*, 2014). We find that depletion of UNC-70/β using the null allele or RNAi results in significant disruption to spermathecal contractility. Both perturbations increase the percentage of spermathecae occupied by an intact or pinched oocyte compared with WT animals fed control RNAi (Figure 3).

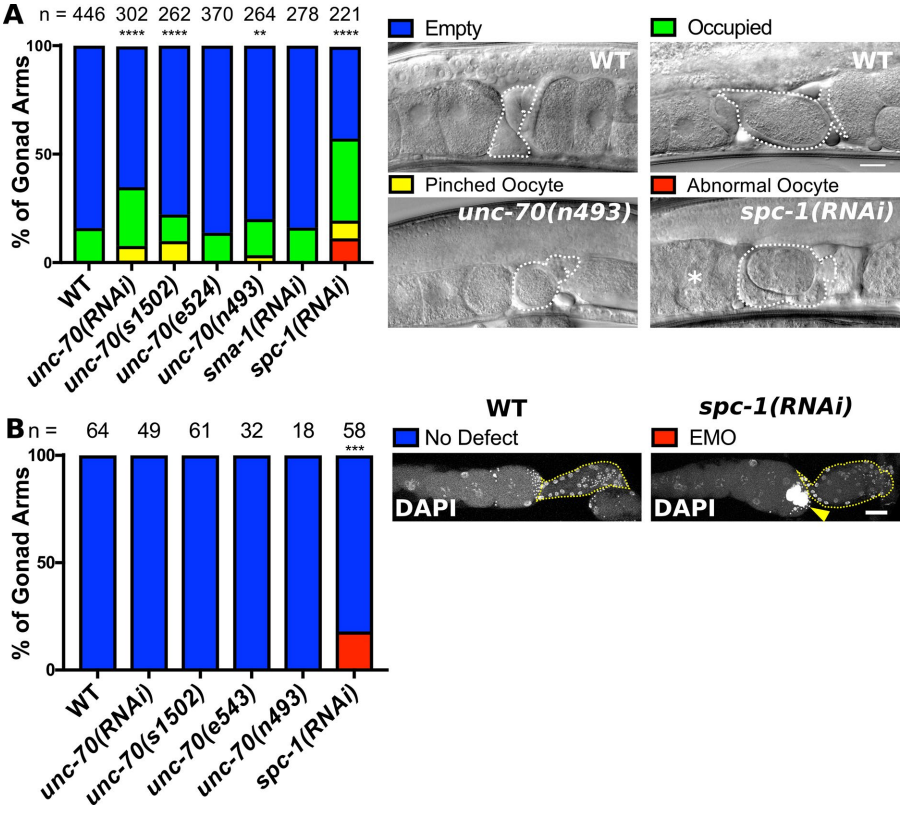

FIGURE 3: Disruption of the spectrin-based membrane skeleton (SBMS) results in ovulation defects. (A) Scoring of gonad contractility defects in animals with disrupted SBMS either by RNAi or the use of alleles. *unc-70(s1502)* is a null allele and *unc-70(e524)* and *unc-70(n493)* are point mutations predicted to disrupt the ability of UNC-70/β to bind SPC-1/α. Example spermathecae that are empty, occupied with an intact oocyte/embryo, occupied with a pinched oocyte, and one gonad with abnormal oocytes are indicated (asterisk). (B) Gonad scored for the EMO phenotype, which was detected using DAPI to label DNA. The spermatheca is indicated by a yellow dashed line in each image. Animals with an EMO phenotype have abnormal, highly polyploid oocytes (yellow arrow). Scale bar, 20 μm. (A) Chi-square test, (B) Fisher's exact test *p* value: $^{**}p \leq 0.01$, $^{***}p \leq 0.001$, $^{****}p \leq 0.0001$. *n* = number of gonads scored.

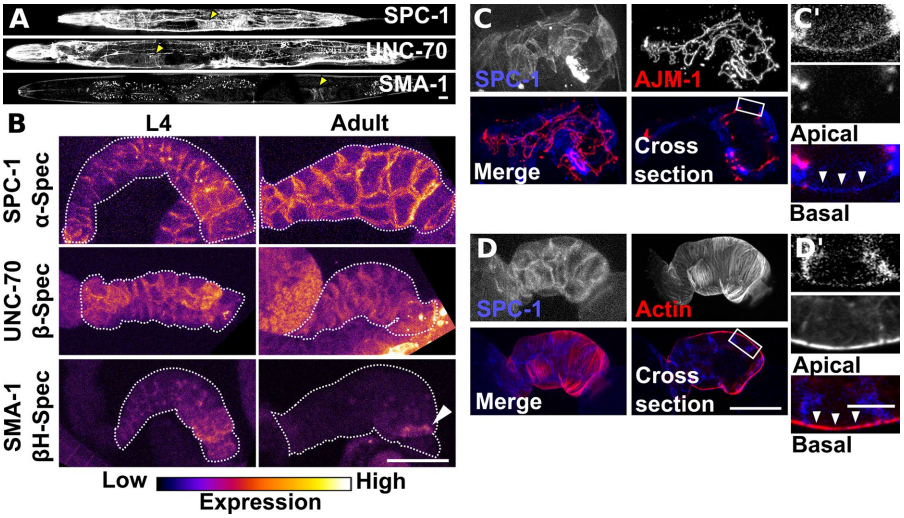

FIGURE 4: SPC-1/alpha-spectrin, UNC-70/β-spectrin and SMA-1/β heavy-spectrin have distinct expression patterns in the spermatheca and SP-UT valve. (A) Confocal maximum intensity projections of whole animals expressing labeled SPC-1/α, UNC-70/β, and SMA-1/βH. Yellow arrow indicates location of the spermatheca. (B) Confocal maximum intensity projections of excised and fixed spermatheca from L4 and young adult animals expressing labeled SPC-1/α, UNC-70/β, and SMA-1/βH. The spermatheca and SP-UT valve are outlined with a dashed line. Note SMA-1/βH is restricted to a band connecting the spermathecal bag and SP-UT valve in the adult spermatheca (white arrow). Images are colored to highlight differences in fluorescence intensity. (C) Confocal maximum intensity projection and a sagittal cross-section of a spermatheca expressing labeled SPC-1/α and AJM-1 to label apical junctions. (C′) Insert from the cross-section in C indicated by a white box with apical at the top and basal at the bottom. SPC-1/α is most prominent at the lateral cell membrane and extends down to the apical junction. A thin layer of SPC-1/α is visible at the basal cell surface (white arrowheads). (D) Confocal maximum intensity projection and a sagittal cross-section of a spermatheca expressing labeled SPC-1/α and GFP::UtrCH to label F-actin. (D′) Insert from the cross-section in D with apical at the top and basal at the bottom. The thin layer of SPC-1/α at the basal cell surface overlaps with basal actin bundles (white arrowheads). Scale bars, 20 μm, 10 μm in inserts.

Milder defects were observed for *unc-70(n493)*, whereas *unc70(e542)* did not differ statistically from WT (Figure 3). We did not detect any defect in *sma-1(RNAi)* animals. This suggests that expression of GFP labeled actin may partially sensitize the spermatheca to disruption of spectrin. However, depletion of SPC-1/α does result in more profound ovulation defects than depletion of either UNC-70/β or SMA-1/βH alone (Figure 3, A and B). In these animals, we frequently observe the accumulation of abnormal oocytes in the proximal gonad (Figure 3A). This phenotype is not observed for depletion of UNC-70/β or SMA-1/βH (Figure 3A). Staining with 4′,6-diamidino-2-phenylindolea (DAPI) suggests that these abnormal oocytes are endomitotic oocytes (EMO) with large abnormal nuclei (Figure 3B). The EMO phenotype occurs when spermathecal entry defects lead to retention of mature oocytes in the proximal gonad where they undergo multiple rounds of abnormal mitosis becoming highly polyploid with large nuclei (Iwasaki *et al.*, 1996). Overall, these findings show that spectrin is required for robust spermathecal contractions that reliably drive exit of embryo through the SP-UT valve and into the uterus ~150 times throughout the adult life of the animal during successive rounds of ovulation.

UNC-70/β- and SMA-1/β heavy-spectrin have unique expression patterns and complementary roles in the spermatheca and SP-UT valve

To better understand the complementary roles of the two β-spectrin isoforms and to determine the subcellular localization of spectrin in the spermatheca, we used transgenic lines expressing labeled SPC-1/α, UNC-70/β, or SMA-1/βH. Prominent UNC-70 expression in the spermatheca has been described previously using an UNC-70/β-specific antibody (Moorthy *et al.*, 2000). However, a translational reporter failed to reproduce this expression pattern (Krieg *et al.*, 2014). The *unc-70* gene is alternatively spliced to generate four isoforms, a–d. The translational reporter described previously (Krieg *et al.*, 2014) reports the expression of isoforms a, b, and d only. To characterize spermathecal expression, and to monitor *unc-70* expression during spermathecal development, we designed a construct that reports the expression of all four *unc-70* isoforms (Supplemental Figure 3). This construct results in an expression pattern (Figure 4A) that closely matches the antibody results reported previously (Moorthy *et al.*, 2000). Strong expression of UNC-70/β in the spermatheca and SP-UT valve begins early in spermathecal development during larval stage 4 (L4) and continues into adulthood (Figure 4B). This suggests isoform UNC-70c is the dominant isoform expressed in the spermatheca. UNC-70c is predicted to use an alternative start codon resulting in the expression of a protein with a unique 103-amino-acid extension just N-terminal to the CH domains (Supplemental Figure 3).

The expression pattern for UNC-70/β closely matches the expression pattern of SPC-1/α (Figure 4, A and B). SPC-1/α expression was determined using a CRISPR generated line that labels the endogenous *spc-1* locus with a C-terminal mKate2 tag. Labeled SPC-1/α is functional and animals expressing SPC-1::mKate2 ovulate similarly to WT (Supplemental Figure 4). As with UNC-70/β, SPC-1/α is prominently expressed in both the spermatheca and SP-UT valve beginning in L4 and extending into adulthood (Figure 4B). In adults, SPC-1/α is also faintly expressed in the sheath (Supplemental Figure 5). To determine the expression pattern of SMA-1/βH, we used a low-copy integrated line expressing the first 3.6 kb of *sma-1* coding sequence in frame with GFP with the *sma-1* promoter and regulatory sequences described previously (Praitis *et al.*, 2001, 2005). SMA-1/βH has a more restricted expression pattern than UNC-70/β (Figure 4, A and B). Beginning in L4, SMA-1/βH is seen in both the spermathecal bag and SP-UT valve with the strongest expression in the four cells most proximal to the SP-UT valve (Figure 4B). Interestingly, this expression pattern changes during spermathecal development, and by adulthood, SMA-1/βH becomes restricted to a ring connecting the spermathecal bag and SP-UT valve (Figure 4B).

To determine the subcellular localization of spectrin, we generated lines coexpressing labeled SPC-1/α and AJM-1::tagRFP, to visualize apical junctions, or GFP::UtrCH, to label F-actin. UNC-70/β has identical subcellular localization to SPC-1/α, so only the results for SPC-1/α are presented here. In adults, the spectrin cytoskeleton, composed of UNC-70/β and SPC-1/α, is most prominent at lateral cell junctions extending from the apical junction marker, AJM-1, to the basal surface (Figure 4C). There is also a thinner layer of spectrin at the basal cell surface that overlaps with the basal, contractile, actomyosin bundles (Figure 4D). This localization pattern is observed

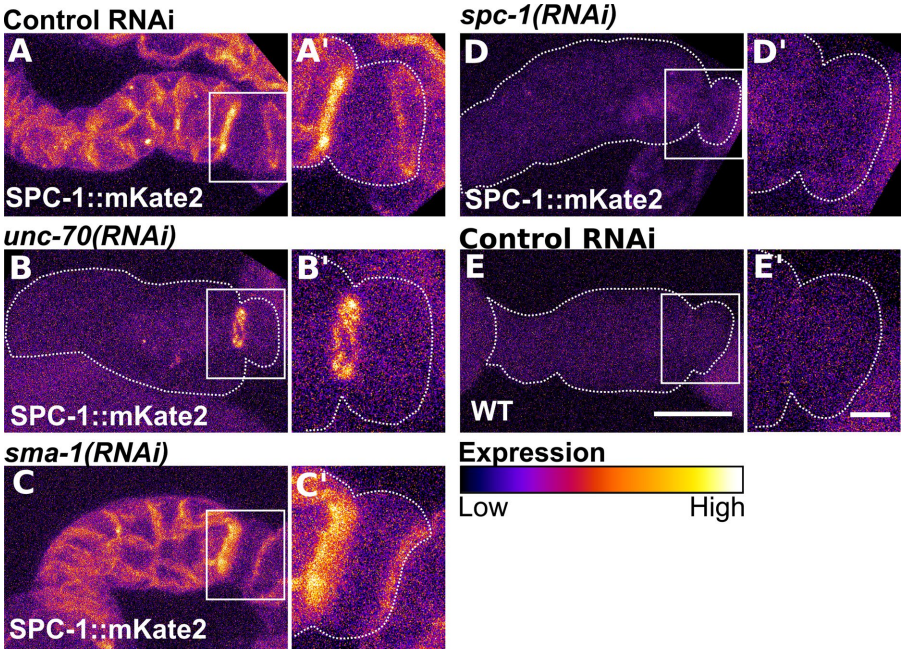

FIGURE 5: The localization of SPC-1/alpha-spectrin requires UNC-70/β-spectrin in the spermathecal bag and both β-spectrin isoforms in the valve. Confocal maximum projections of excised and fixed spermathecae from animals expressing SPC-1/α with a CRISPR generated mKate2 tag at the endogenous locus (SPC-1::mKate2) treated with control RNAi (A), RNAi against *unc-70* (B), *sma-1* (C), and *spc-1* (D). Note the loss of SPC-1/α at spermathecal cell boundaries with depletion of UNC-70/β (B) but retention of SPC-1/α in a band connecting the spermathecal bag and SP-UT valve (B′). SPC-1/α localization is not changed with SMA-1/βH depletion (C–C′). (E) Confocal maximum projections of an excised and fixed spermatheca from a WT, unlabeled, animal appears similar to the SPC-1::mKate2 line treated with RNAi against *spc-1* in D. Inserts in A′–E′ are a magnified view of the valve indicated by a white box in A–E. Images are colored to highlight differences in fluorescence intensity. Scale bars, 20 μm, 5 in inserts.

in young adult animals prior to the first ovulation and is maintained throughout adulthood.

Because the interaction between β- and α-spectrin is required for maintenance of α-spectrin protein expression (Hulsmeier *et al.*, 2007) and the formation of tetramers that cross-link actin (Li *et al.*, 2008, 2010), we hypothesized that the expression level and or localization of SPC-1/α would require one or both of the two β-spectrin isoforms. To determine this, we used RNAi to deplete UNC-70/β in the CRISPR line expressing a labeled SPC-1/α. With depletion of UNC-70/β, SPC-1/α is no longer clearly visible along cell boundaries of the spermathecal bag cells, suggesting SPC-1/α may be degraded in the absence of UNC-70/β (Figure 5B). It is also possible that diffuse cytosolic localization of SPC-1/α in the absence of UNC-70/β is below the limit of detection. Interestingly, SPC-1/α is maintained in a ring connecting the spermathecal bag and SP-UT valve in the absence of UNC-70/β (Figure 5B). This corresponds with the localization pattern of SMA-1/βH (Figure 4B). To determine whether SMA-1/βH depletion impacts SPC-1/α expression, we performed the same experiment knocking down *sma-1* rather than *unc-70*. Consistent with the milder contractility defects observed with *sma-1(RNAi)* compared with *unc-70(RNAi)* (Figures 2C and 3A), we find that loss of SMA-1/βH does not result in observable alterations to SPC-1/α localization (Figure 5C). RNAi of *spc-1* results in complete loss of detectable SPC-1::mKate2 fluorescence with fluorescence levels similar to what is seen in unlabeled WT, N2, animals (Figure 5, D and E).

Spectrin is required for robustness and orientation of central actomyosin bundles

To determine whether disruption to actomyosin bundle organization contributes to the contractility defects observed with UNC-70/β and SPC-1/α depletion, we used phalloidin to visualize F-actin on the basal surface of excised and fixed gonads. In mature WT animals that have experienced ovulations, each spermathecal cell contains 8.2 ± 1.9 (mean ± SD; n = 32 cells) prominent parallel actin bundles at the basal cell surface, termed central actin bundles, that are not clearly distinguishable from actin bundles that run along the basal cell edges, termed peripheral actin bundles (Figure 6, A–C). These central actin bundles are oriented along the long axis of each cell (Figure 6C). In spermathecal cells with disrupted spectrin, either through depletion of UNC-70/β or SPC-1/α, the central actin bundles are diminished both in number and intensity, and the peripheral actin bundles appear more prominent (Figure 6, A–C). This is also true for the two alleles of *unc-70* that are predicted to affect regions of UNC-70/β required for tetramerization with SPC-1/α, *unc-70(e524)* and *unc-70(n493)* (Figure 6, A–C). In close agreement with the quantification of spermathecal contractility defects (Figure 3A), we find that *unc-70(e524)* and *unc-70(n493)* result in less severe actin defects than the null allele or *unc-70(RNAi)* (Figure 6, A–C). We find that the *unc-70(n493)* allele has a stronger actin defect than the *unc-70(e524)* allele producing fewer actin bundles and bundles that are less prominent (Figure 6, A–C). The *unc-70(n493)* allele also results in a more severe contractility defect than the *unc-70(e524)* allele (Figure 3A). This indicates a close relationship between actin organization and spermathecal contractility.

As expected, knockdown of SPC-1/α and UNC-70/β result in similar actin phenotypes (Figure 6, A–C). Both the number and intensity of central actin bundles are reduced in *spc-1(RNAi)* cells. However, the *spc-1(RNAi)* actin phenotypes are more variable, possibly due to penetrance of the RNAi (Figure 6, A and B). We occasionally observe defects in actin bundle distribution and orientation in *spc-1(RNAi)* and *unc-70(RNAi)* spermathecae (Figure 6, D and E). In cells with actin bundle orientation defects, the actin bundles within a cell are aligned but run perpendicular to the long cell axis (Figure 6, D and E). Neighboring cells in these spermathecae retain the expected orientation with actin bundles parallel to the long cell axis (Figure 6, D and E). This phenotype is rare and seen only in spermathecal cells with disrupted spectrin that still produce prominent actin bundles. This phenotype is not seen with strong loss of UNC-70/β function using the null allele, suggesting the phenotype results from partial knockdown of spectrin genes.

In addition to disruption of actin in the spermathecal bag cells, we also observe defects in actin organization in the SP-UT valve (Figure 4, A–C). In WT animals, the SP-UT valve contains a dense actin network at the apical surface. When the valve is closed, this dense network forms a continuous tube where individual actin bundles are not distinguishable except at the most proximal point of

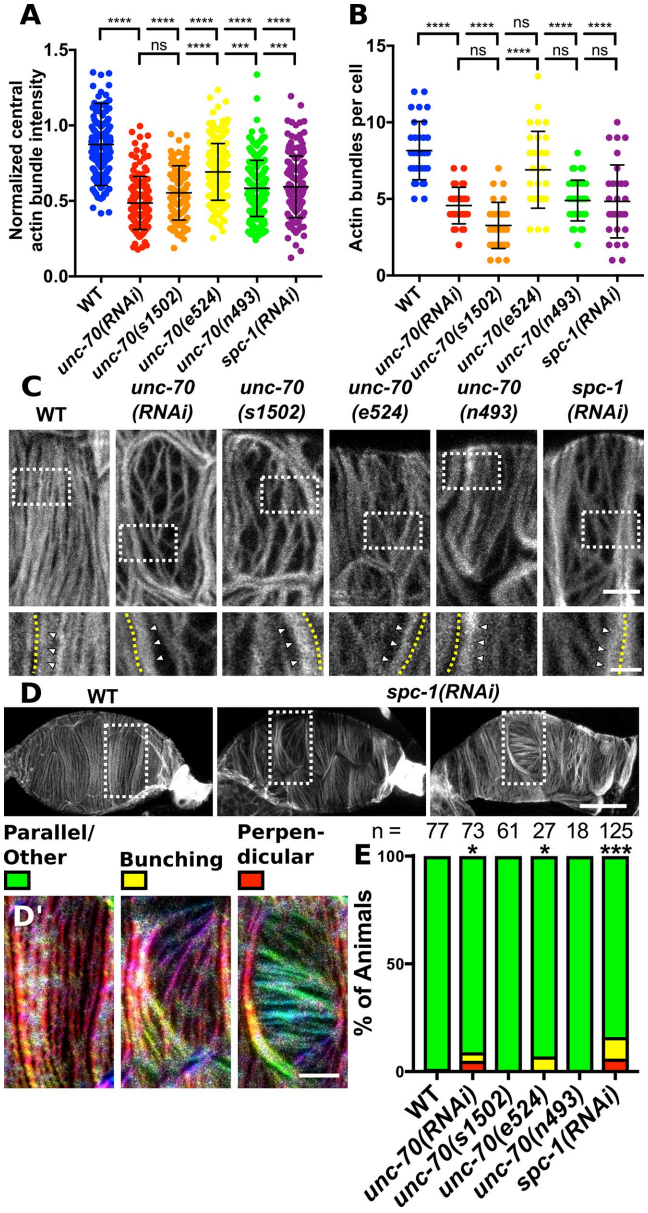

FIGURE 6: Spectrin is required for prominent central actin bundles and actin bundle orientation. Basal F-actin is visualized using phalloidin staining in excised and fixed spermathecae. Images are of confocal maximum intensity projections. (A) Quantification of central actin bundle intensity normalized to actin intensity at the cell periphery for WT spermathecal cells and cells with disrupted SBMS using RNAi or alleles. Each point is the measurement of a single actin bundle. (B) Quantification of the number of central actin bundles in each cell. Each point represents a single cell. Measurements in A and B are from the same cells. For each measurement, WT $n = 264$ actin bundles from 31 individual cells (13 animals), *unc-70(RNAi)* $n = 140$ actin bundles from 30 individual cells (12 animals), *unc-70(sb105)* $n = 98$ actin bundles from 30 individual cells (13 animals), *unc-70(cb542)* $n = 205$ actin bundles from 30 individual cells (12 animals), *unc-70(n493)* $n = 186$ bundles from 31 individual cells (12 animals), and *spc-1(RNAi)* $n = 150$ bundles from 31 individual cells (12 animals). In all cases, no more than 3 cells were measured from the same animal. Error bars represent SD. Dunnett's multiple comparison test p value: ns $p > 0.05$, ***$p \leq 0.001$, ****$p \leq 0.0001$. (C) Representative images of the cells analyzed in A and B. Inserts in C are indicated with a white dashed box. Within inserts, the cell boundary is indicated with a yellow dashed. Peripheral actin bundles (white arrowheads) appear brighter than central actin bundles in cells with disrupted SBMS. (D) Representative images of WT and *spc-1(RNAi)* spermathecae with bunched (left) and perpendicular (right) actin bundles. (D′) Magnified inserts from the area in D indicated by a white box. Inserts are colored using OrientationJ where warm colors indicate vertical bundles and cooler colors indicate horizontal bundles. (E) Quantification of scoring for the bunched and perpendicular actin bundle phenotype in individual spermathecae. Chi-square test, p value: *$p \leq 0.05$, ***$p \leq 0.001$. n = number of spermathecae scored. Scale bars, 5 μm in C, 2 μm in the inserts in C, 20 μm in D, and 5 μm in D′.

the valve where fine actin bundles extend outward toward the uterus (Figure 7B). When the valve is partially open, this dense network is expanded, and individual actin bundles are more clearly distinguishable (Figure 7B). However, even in open valves, the SP-UT valve actin network remains interconnected and attached to the spermathecal bag (Figure 7B). In *spc-1(RNAi)* animals, the SP-UT valve actin network frequently appears torn and partially disconnected from the spermathecal bag (Figure 7, A and C). This valve defect is not observed in UNC-70/β-depleted animals (Figure 7A) consistent with our observation that UNC-70/β and SMA-1/βH are both expressed and appear to act redundantly in the valve (Figures 4B and 5, B and C). Interestingly, this valve defect is only observed in *spc-1(RNAi)* animals that have undergone an ovulation suggesting that valve tearing may result from mechanical stress during ovulation (Figure 7A). While we do find faint SPC-1/α expression in the sheath, knockdown of *spc-1* or *unc-70* does not notably alter F-actin organization in sheath cells (Supplemental Figure 5). Collectively, these results indicate spectrin contributes to spermathecal contractility through influencing organization of the contractile actomyosin machinery.

Spectrin is required for maintenance of central actin bundles postdevelopment

To determine whether spectrin plays a role in maintaining central actin bundles postdevelopment, we used the auxin-inducible decay (AID) system to deplete SPC-1/α at different time points. AID allows for spatiotemporally regulated degradation of degron-tagged proteins on exposure to the plant phytohormone auxin (Zhang *et al.*, 2015). In the presence of auxin, the plant-derived F-box protein, TIR1, specifically binds to the degron peptide and recruits endogenous E3 ubiquitin ligase complex components leading to ubiquitination and proteasome degradation of the degron-tagged protein (Nishimura *et al.*, 2009). We expressed TIR1 under the control of a spermathecal-specific promoter in the background of the CRISPR-generated line expressing *spc-1::degron::mKate2* from the endogenous locus. These animals also express GFP::UtrCH in the spermatheca to label F-actin. TIR1 was fused to a histone mCherry marker with a cleavable F2A peptide allowing us to use mCherry::H2B expression to track expression of the unlabeled TIR1 protein. Expression of TIR1 in the absence of auxin has no effect on spermathecal actin organization and does not result in depletion of SPC-1/α (Figure 8, A–C). The *fln-1* promoter driving *TIR1::F2A::mCherry::H2B* turns on in the spermatheca during early L4 (Kovacevic and Cram, 2010). Therefore, animals grown continuously in the presence of auxin begin to degrade degron-tagged SPC-1/α during L4. By adulthood, SPC-1::degron::mKate2 levels in these animals are below the limit of detection in the spermatheca, and spermathecal central actin bundles are diminished in number and intensity (Figure 8, A–C). This result is similar to what is seen with depletion of *spc-1* using RNAi, indicating the AID system effectively depletes SPC-1/α specifically on addition of auxin.

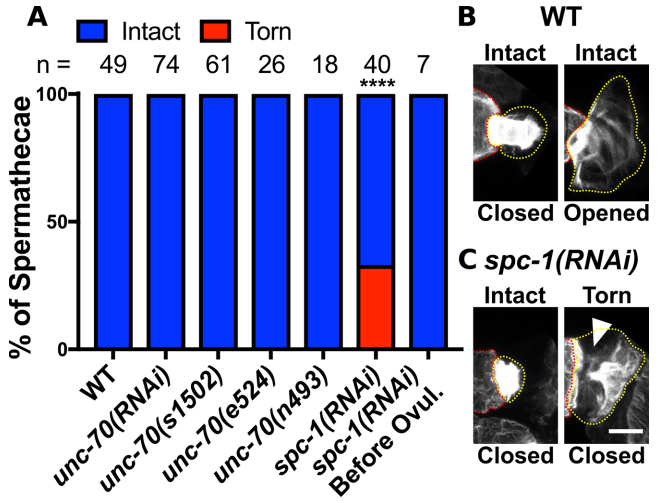

FIGURE 7: UNC-70/β-spectrin and SMA-1/β heavy-spectrin cooperate with SPC-1/α-spectrin to maintain F-actin attachment in the SP-UT valve. (A) Quantification of spermathecae scored for SP-UT valve actin defects on disruption of the SBMS. The SBMS is disrupted by either RNAi depletion of spectrin or the use of alleles. (B, C) F-actin is visualized in fixed and excised spermathecae using phalloidin staining (grayscale). Images are confocal maximum intensity projections. (B) Examples of intact closed and opened valves from WT spermathecae. (C) Examples of valves from animals treated with *spc-1* RNAi. Before the first ovulation *spc-1(RNAi)* SP-UT valves are intact and after ~30% appear torn. In torn valves, part of the actin network pulls away from the spermathecal bag (white arrow). The spermathecal bag is indicated with a red dashed line and the valve is outlined in a yellow dashed line. Scale bar, 5 μm. Fisher's exact test *p* value: ****$p \leq 0.0001$. *n* = number of gonads scored.

To determine the role of SPC-1/α postdevelopment, we exposed TIR1-expressing adult animals to auxin at different time points. Animals were treated with auxin as young adults just before the first ovulation and as mature adults that had undergone approximately two to five ovulations. Animals treated as young adults have completed the cell division and migration events that occur during gonad morphogenesis (Hubbard and Greenstein, 2000) and begin degrading SPC-1/α around the time of the first ovulation when central spermathecal actin bundles are forming (Wirshing and Cram, 2017). The spermathecal cells of these animals have disrupted actin bundles that are diminished in number and intensity compared with untreated controls (Figure 8, A–C). However, the diminished actin bundle phenotype is less severe in animals treated with auxin as young adults compared with those that begin degrading SPC-1/α during L4 (Figure 8, A–C). Animals treated with auxin as mature adults post the first ovulation begin degrading SPC-1/α after development of central spermathecal actin bundles. These animals also show defects in spermathecal actin and have fewer and less prominent central actin bundles (Figure 8, A–C). Overall, these results indicate a role for spectrin in maintaining central actin bundles throughout successive rounds of ovulation in adults.

Spectrin is required for reinforcement of central actin bundles during contraction

We have shown previously that active myosin is recruited to contractile actomyosin bundles in the spermatheca and that the production of prominent parallel bundles coincides with and requires contraction (Wirshing and Cram, 2017; Kelley *et al.*, 2018). To determine whether myosin recruitment to actomyosin bundles or bundle dynamics during contraction is altered by depletion of spectrin, we used fluorescently labeled proteins to visualize actin and myosin and time-lapse confocal microscopy. In the following experiments, we show the results obtained for knockdown of UNC-70/β only, because UNC-70/β and SPC-1/α appear to be mutually required in the spermathecal bag and depletion of either produces similar results.

Colabeling of F-actin and myosin using the moesin actin-binding domain fused to mCherry (MoeABD::mCherry) to label F-actin and myosin tagged with GFP (GFP::NMY-1) shows that actin and myosin colocalize into basal actomyosin bundles (Supplemental Figure 6). In agreement with our phalloidin staining results, these bundles are prominent in WT cells and appear less prominent in *unc-70(RNAi)* cells (Supplemental Figure 6). As seen in excised and fixed spermathecae, UNC-70/β depletion results in a loss of central actomyosin bundles and more prominent actin at the cell periphery (Supplemental Figure 6). However, in both WT and *unc-70(RNAi)* cells, actin and myosin colocalize into basal bundles, suggesting spectrin is not required for activation and recruitment of myosin into actomyosin bundles.

Because spectrin is required postdevelopment to maintain actin bundles, we wanted to determine whether cell stretch or contraction during ovulation contribute to diminished actin bundles in cells with disrupted spectrin. We used time-lapse confocal microscopy to monitor spermathecal actin bundles during ovulation in animals expressing GFP labeled actin. In WT cells immediately after oocyte entry, central bundles are less prominent than actin at the cell periphery (Figure 9, A and B, and Supplemental Movie 1). These central bundles become more prominent during contraction (Figures 9, A and B, and 10, A and B). Spermathecal cells treated with *unc-70(RNAi)* are similar to WT at the start of ovulation (Figure 9, A and B, and Supplemental Movie 1). However, in these cells central actin bundles diminish in intensity during ovulation and become less prominent than actin at the cell periphery (Figures 9, A and B, and 10, A and B, Supplemental Movie 1). To determine whether contraction during ovulation is required to drive thinning of the central bundles, we used the null allele of *plc-1*, *plc-1(rx1)*. PLC-1 is required for the production of Ca^{2+} transients during ovulation (Kovacevic *et al.*, 2013) that activate the myosin light chain kinase, MLCK-1, increase myosin activity, and drive contraction (Kelley *et al.*, 2018). RNAi knockdown of *unc-70* in the *plc-1(rx1)* background attenuates the diminished central actin bundle phenotype (Figure 10, A–C). In these spermathecal cells, there is a slight but not significant reduction in central actin during ovulation (Figure 10C). The *plc-1(rx1);unc-70(RNAi)* actin phenotype is similar to the *plc-1(rx1)* actin phenotype (Figure 10, A–C). This suggests actomyosin contraction contributes to bundle thinning in spermathecal cells with disrupted spectrin.

DISCUSSION

Spectrin influences spermathecal contractility and actin network organization

Here we describe a novel screening approach designed to identify actin interacting and regulatory genes required for *C. elegans* spermathecal contractility. With this approach we identify six genes required for robust spermathecal contractility, including two we have previously characterized in the spermatheca encoding nonmuscle myosin II, NMY-1 (Kovacevic *et al.*, 2013; Wirshing and Cram, 2017), and filamin, FLN-1 (Kovacevic and Cram, 2010; Kovacevic *et al.*, 2013), as well as the components of the spectrin cytoskeleton that we characterize in this work. *Caenorhabditis elegans* has three spectrin genes, *spc-1*, *unc-70,* and *sma-1*, encoding α-spectrin, β-spectrin, and β heavy-spectrin, respectively. While all three genes influence ovulation, the two beta isoforms,

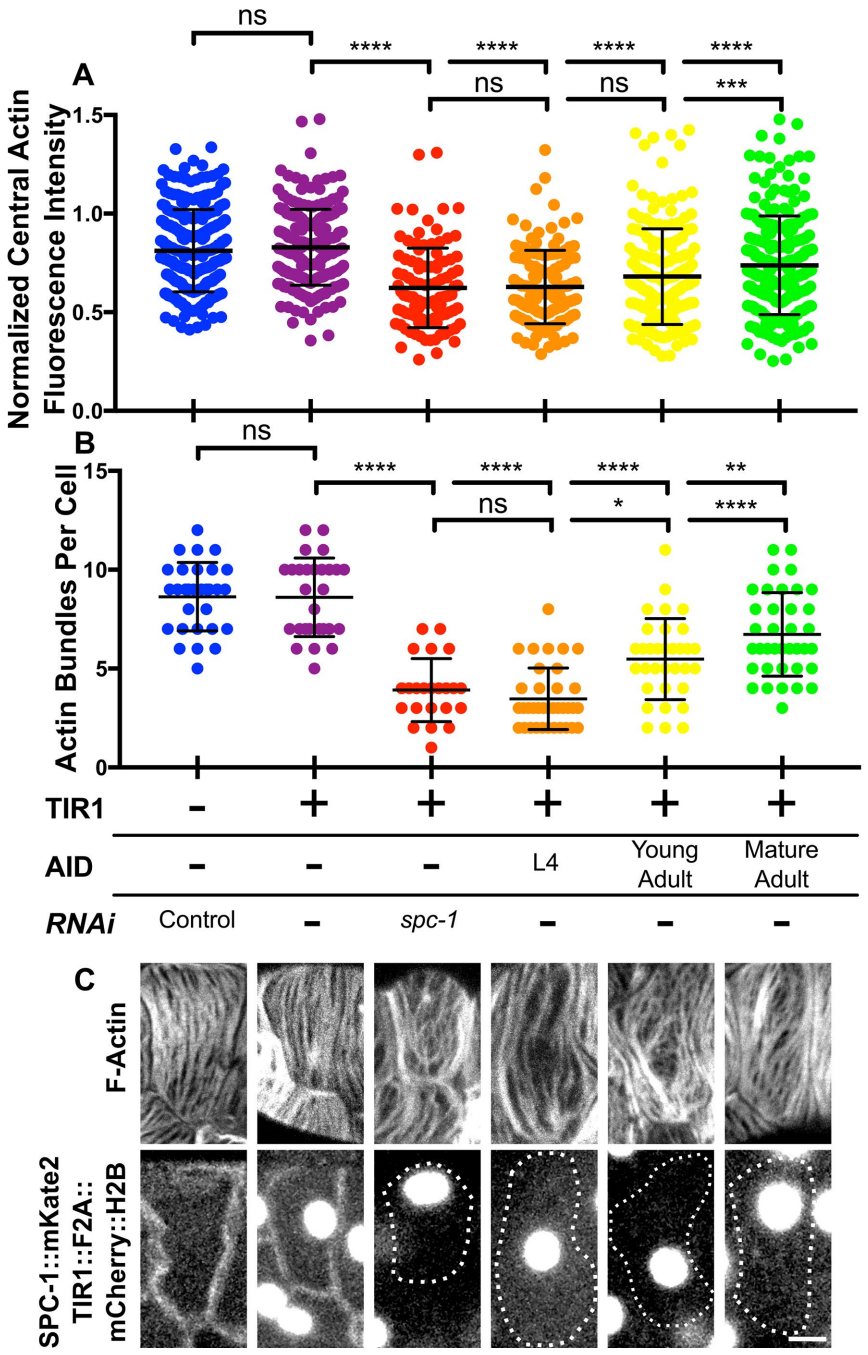

FIGURE 8: The SBMS is required for maintenance of central actin bundles postdevelopment. (A) Quantification of central actin bundle intensity normalized to actin intensity at the cell periphery for WT spermathecal cells and cells with disrupted SBMS using RNAi or AID to deplete SPC-1/α. Each point is the measurement from a single actin bundle. (B) Quantification of the number of central actin bundles in each cell. Each point represents a single cell. Measurements in A and B are from the same cells. For the control condition without AID $n = 259$ bundles from 30 cells (14 animals), for TIR1 expressing animals without AID $n = 217$ bundles from 28 cells (12 animals), for *spc-1(RNAi)* condition $n = 104$ bundles from 30 cells (14 animals), for AID starting at L4 $n = 130$ bundles from 23 cells (14 animals), AID starting at young adulthood $n = 172$ bundles from 33 cells (14 animals), and for AID starting at mature adulthood $n = 255$ bundles from 37 cells (14 animals). For all conditions, no more than three cells were measured from the same animal. (C) Representative cells for the data presented in A and B. F-actin is labeled using GFP::UtrCH and SPC-1/α is labeled with mKate2. TIR1 is fused to mCherry::H2B nuclear marker with an F2A peptide to track TIR1 expression. In cells without SPC-1/α, cell outlines are indicated with a dashed line. Error bars represent SD. Dunnett's multiple comparison test p value: ns $p > 0.05$, *$p \le 0.05$, **$p \le 0.01$, ***$p \le 0.001$, ****$p \le 0.0001$. Scale bar, 5 μm.

UNC-70/β and SMA-1/βH, have distinct expression patterns and roles. SPC-1/α and UNC-70/β are broadly expressed in the spermatheca throughout development, while SMA-1/βH expression changes as animals enter adulthood and becomes restricted to a ring joining the spermathecal bag and valve. Similarly, isoform specific expression patterns have been reported in invertebrate (Thomas and Kiehart, 1994; Thomas *et al.*, 1998; Thomas and Williams, 1999; Dubreuil *et al.*, 1997, 2000; McKeown *et al.*, 1998; Moorthy *et al.*, 2000; Médina *et al.*, 2002; Norman and Moerman, 2002) and vertebrate systems (Stankewich *et al.*, 2016), and reorganization of the spectrin cytoskeleton during development and cell response to stress is also seen in *Drosophila* (Thomas and Kiehart, 1994; Thomas *et al.*, 1998; Thomas and Williams, 1999; Dubreuil *et al.*, 2000; Médina *et al.*, 2002), *Xenopus* (Ryabova *et al.*, 1994), and vertebrate systems (Dosemeci and Reese, 1995; Faddis *et al.*, 1997; Lee *et al.*, 2001; Kim *et al.*, 2016). These similarities suggest insights into the roles of spectrin in the spermatheca may be broadly applicable to other systems.

To determine whether spectrin influences spermathecal contractility through regulation of the contractile actomyosin machinery, we observed actin structures in WT and spectrin-depleted cells. Consistent with the expression patterns, UNC-70/β regulates actin morphology in spermathecal bag cells, while both UNC-70/β and SMA-1/βH are required in the valve. In WT spermathecal bag cells, prominent, parallel actin bundles are present on the basal surface of each cell. In contrast, depletion of either SPC-1/α or UNC-70/β results in thin central actomyosin bundles that are less prominent than the actin bundles at the cell periphery. Depletion of SPC-1/α also results in actin in the valve tearing and partially pulling away from the spermathecal bag. Spectrin may function to strengthen actin attachment in the valve through interactions with cell–cell adhesion components as seen in vertebrates (Nelson *et al.*, 1990; Kizhatil *et al.*, 2007) and invertebrates (Zarnescu and Thomas, 1999; Médina *et al.*, 2002). These actin phenotypes are distinct from what we have observed previously in NMY-1-/myosin II-depleted spermathecal cells, which fail to develop prominent, parallel, central bundles (Wirshing and Cram, 2017), or with FLN-1/filamin depletion, which results in complete loss of central bundles (Kovacevic and Cram, 2010). These differences may explain our finding that depletion of either NMY-1/myosin II or FLN-1/filamin results in stronger loss of spermathecal contractility compared with depletion of spectrin. We suggest that spectrin

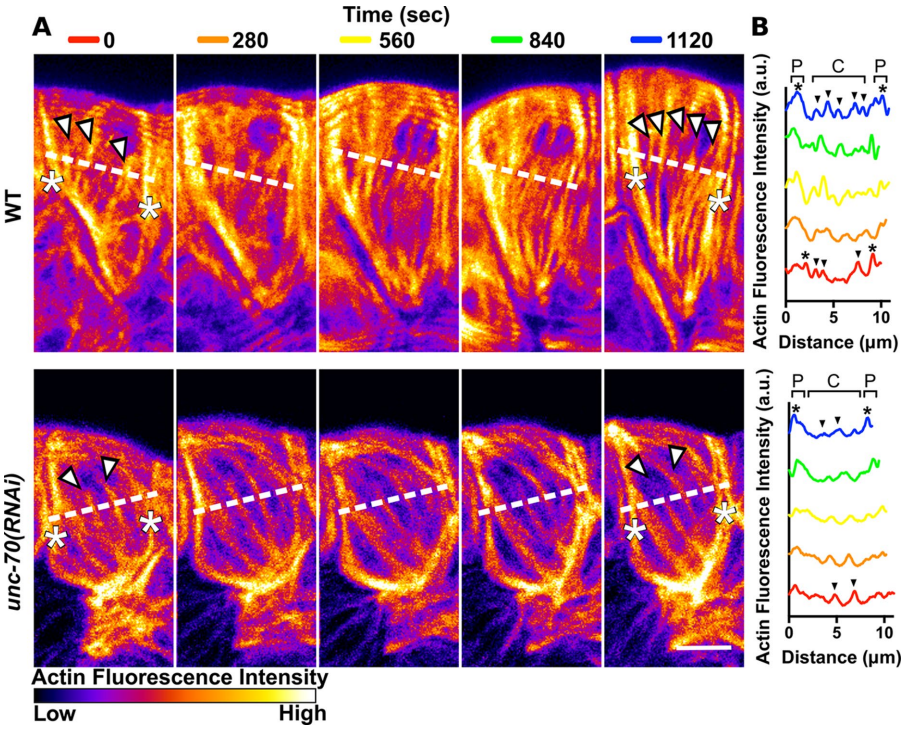

FIGURE 9: Spectrin is required for production of prominent central actin bundles during ovulation. (A) Confocal maximum intensity projections of spermathecae expressing GFP::ACT-1 to label actin. Images are frames from first ovulation movies at 280-s intervals from oocyte entry (0 s) to after contraction (1120 s) colored to highlight differences in fluorescence intensity. In the WT cell before contraction (0 s), three prominent central bundles are seen (white arrows) that appear less bright than actin bundles at the cell periphery (asterisks). During contraction, central actin bundles become more prominent. After contraction (1120 s), at least five prominent central actin bundles are visible (white arrows) that are nearly as bright as actin bundles at the cell periphery (asterisks). In the *unc-70(RNAi)* cell before contraction (0 s), there are two prominent central actin bundles (white arrowheads). These central bundles diminish in intensity during contraction while peripheral bundles are maintained and slightly increase in intensity. After contraction (1120 s), the central bundles (white arrowheads) are less prominent than the bright actin bundles at the cell periphery (asterisks). (B) Quantification of fluorescence intensity of a line drawn across the WT cell and the *unc-70(RNAi)* cell indicated by dashed lines in A. Prominent central bundles are indicated by black arrows and peripheral actin bundles are indicated by black asterisks. Scale bar, 5 μm.

may play a subtler role in fine-tuning actin bundle morphology to allow for robust spermathecal contractility throughout adulthood. Loss of central stress fibers has also been observed in cultured epithelial cells with disrupted spectrin (Metral *et al.*, 2009; Collec *et al.*, 2011). Interestingly, disruption of spectrin in cultured fibroblasts had the opposite effect, resulting in increased central stress fiber production (Stankewich *et al.*, 2011). Given the diversity of spectrin-interacting proteins (Bennett and Baines, 2001; Machnicka *et al.*, 2014) and tissue-specific expression patterns (Stankewich *et al.*, 2016), it is perhaps not surprising that the role of spectrin is context specific.

In addition to reduced central actin bundles, we occasionally observe actomyosin bundles oriented perpendicular to the long cell axis in spectrin-depleted cells. The spectrin cytoskeleton interacts with mechanoperceptive components of cell–cell and cell–ECM adhesion complexes (Nelson *et al.*, 1990; Zarnescu and Thomas, 1999; Kizhatil *et al.*, 2007; Metral *et al.*, 2009; Collec *et al.*, 2011; Ponceau *et al.*, 2015), and spectrin itself can act as a mechanotransducer (Krieg *et al.*, 2014; Wu *et al.*, 2017) and contributes to membrane mechanical properties (Krieg *et al.*, 2014; Smith *et al.*, 2018). Cell culture experiments have shown that actin networks align in response to the magnitude and orientation of cell stretch (Kaunas *et al.*, 2005; Lee *et al.*, 2010a; Sears and Kaunas, 2016). Disruption of spectrin may alter the forces produced and experienced by spermathecal cells as has been reported in *C. elegans* embryos (Vuong-Brender *et al.*, 2017). In support of this hypothesis, the misalignment phenotype is only observed in cells of the main spermathecal bag near the distal neck. We suggest that these cells are more vulnerable to actin bundle misalignment, compared with their central neighbors, due to tissue topography, as this has been shown to regulate actin bundle alignment in *Drosophila* embryos (Chanet *et al.*, 2017).

Spectrin is required for development and maintenance of robust central actin bundles during contraction

We have shown previously that parallel actin bundles in spermathecal cells develop concomitantly with contraction during the first ovulation and that contraction is required to drive actin bundle production (Wirshing and Cram, 2017; Kelley *et al.*, 2018). These actin bundles are maintained throughout adulthood. However, the mechanism allowing for maintenance of robust actin bundles throughout successive rounds of stretch and contraction remained largely unknown. Here we use AID to deplete spectrin in mature adults with well-developed central actin bundles. Using this approach, we find that central actin bundles become diminished, indicating spectrin is required not only for development but also maintenance of central actin bundles. This expands on previous work in *Drosophila* (Dubreuil *et al.*, 1998; Wong *et al.*, 2015), *C. elegans* (Hammarlund *et al.*, 2000; Moorthy *et al.*, 2000; Norman and Moerman, 2002; Praitis *et al.*, 2005), and mouse models (Stankewich *et al.*, 2011; Lim *et al.*, 2014) that has shown that spectrin regulates actin morphology during development and highlights the contribution of spectrin to maintaining actin structures postdevelopment. This role of spectrin may be particularly relevant to the function of spermathecal cells, as these cells withstand numerous cycles of stretch and contraction during ovulation.

To determine when during ovulation central actin bundles become depleted in cells with disrupted SMBS, we use confocal time-lapse microscopy to capture actin dynamics during cell stretch and contraction. We find that central actin bundles in cells with disrupted SMBS become depleted during contraction, while central actin bundles become reinforced in WT cells. Furthermore, we genetically block contraction to show that thinning of central actin bundles in spectrin-depleted cells is driven by contraction. Both cell culture (Medeiros *et al.*, 2006) and in vitro (Molloy *et al.*, 1995; Haviv *et al.*, 2008; Lenz *et al.*, 2012) experiments have shown myosin is capable of producing forces that break and depolymerize F-actin. In other systems, mechanoperceptive proteins at cell–cell and cell–ECM junctions increase F-actin recruitment and anchorage to strengthen actin networks under myosin-induced tension (Humphries *et al.*, 2007;

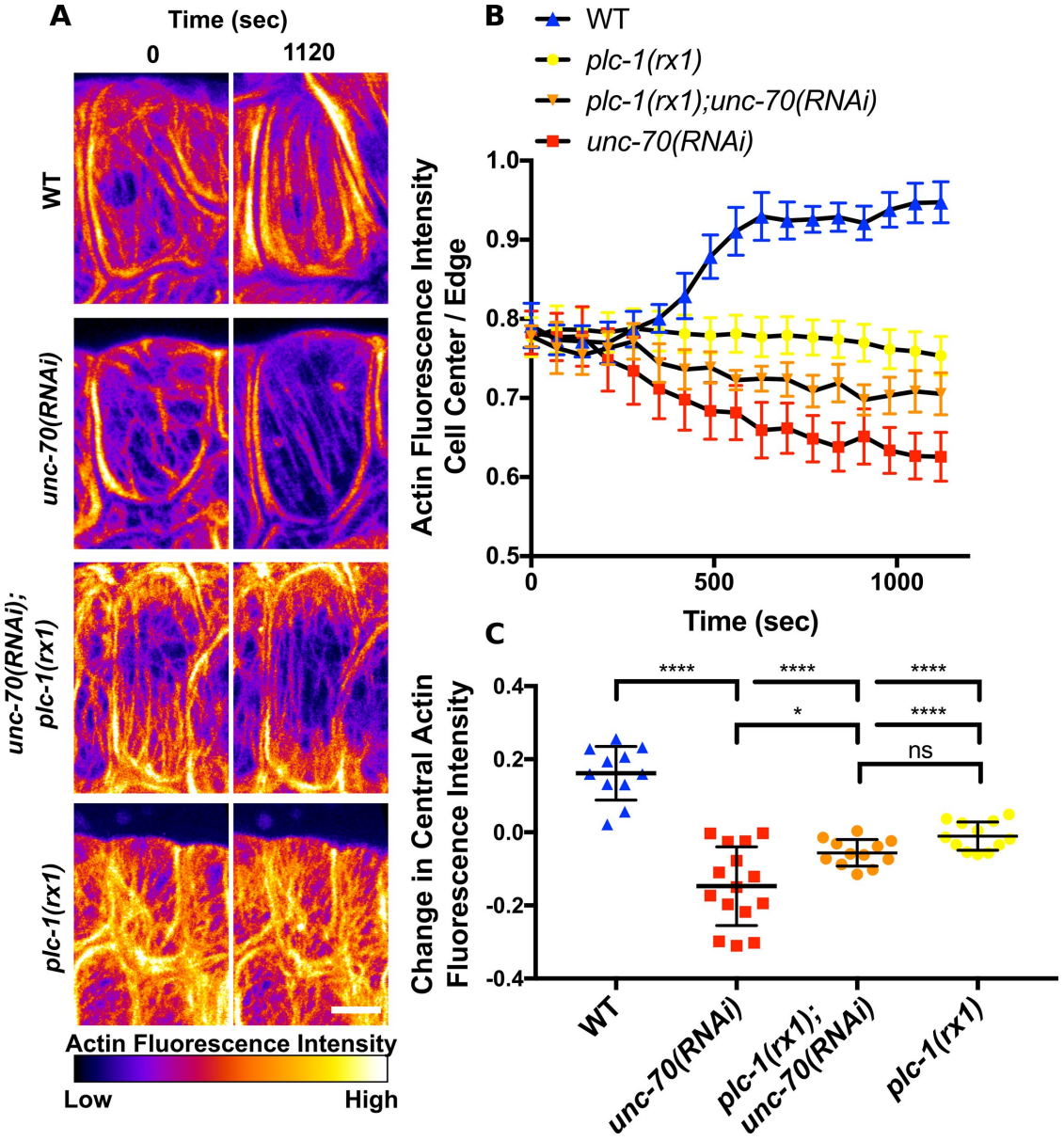

FIGURE 10: Spectrin maintains central actin bundles during contraction. (A) Confocal maximum intensity projections of spermathecae expressing GFP::ACT-1 to label actin. Images are frames from first ovulation movies on oocyte entry (0 s) and after contraction (1120 s). Images are colored to highlight differences in fluorescence intensity. In the WT cell (first row), central actin bundles become more prominent after contraction. In the *unc-70(RNAi)* cell (second row), central actin bundles diminish and actin at the cell periphery appears more prominent. This decrease in central actin fluorescence intensity with RNAi of *unc-70* is mitigated in a background with genetically ablated Ca^{2+} signaling, expressing the *plc-1* null allele, *plc-1(rx1)* (third row). In the cell expressing *plc-1(rx1)* without RNAi knockdown of *unc-70* (fourth row), there is no net change in actin fluorescence intensity. (B) Quantification of central actin bundle fluorescence normalized to actin fluorescence at the cell periphery at 70 s intervals during ovulation. (C) Quantification of the change in normalized central actin bundle fluorescence during ovulation. Normalized actin bundle intensity increases in WT cells, decreases in *unc-70(RNAi)* cells, and remains the same in *plc-1(rx1)* cells with and without RNAi knockdown of *unc-70* during ovulation. The same cells were analyzed in B and C. For WT $n = 10$ cells (four ovulation movies), for *unc-70(RNAi)* $n = 9$ cells (four ovulation movies), for *plc-1(rx1);unc-70(RNAi)* $n = 12$ cells (four ovulation movies), and for *plc-1(rx1)* $n = 12$ cells (four ovulation movies). No more than three cells were measured from the same movie. Error bars indicate SEM in B and SD in C. Dunnett's multiple comparison test p value: ns $p > 0.05$, *$p \leq 0.05$, ****$p \leq 0.0001$. Scale bar, 5 μm.

Yonemura *et al.*, 2010; Leerberg *et al.*, 2014; Higashi *et al.*, 2016). Spectrin interacts with cell–cell (Nelson *et al.*, 1990; Zarnescu and Thomas, 1999; Kizhatil *et al.*, 2007) and cell–ECM adhesion complexes (Metral *et al.*, 2009; Ponceau *et al.*, 2015) and may act through these complexes to influence actin bundle maintenance. Additionally, spectrin interacts with tropomyosin (Tang *et al.*, 2003). In *C. elegans* body wall muscles and sheath cells, tropomyosin/LEV-11 stabilizes F-actin and protects F-actin from cleavage by

ADF/cofilin/UNC-60 (Ono and Ono, 2004; Ono *et al.*, 2007; Yu and Ono, 2006). Tropomyosin/LEV-11 and ADF/cofilin/UNC-60 are also expressed in the spermatheca where they may play similar roles (Ono *et al.*, 2003, 2007).

Conclusion

Work in vivo has elucidated the roles of spectrin in morphogenesis and development both in vertebrates (Tang *et al.*, 2003; Stankewich *et al.*, 2011; Lim *et al.*, 2014) and invertebrates (Thomas and Kiehart, 1994; Thomas *et al.*, 1998; Thomas and Williams, 1999; de Cuevas *et al.*, 1996; Dubreuil *et al.*, 1998; McKeown *et al.*, 1998; Zarnescu and Thomas, 1999; Hammarlund *et al.*, 2000; Moorthy *et al.*, 2000; Médina *et al.*, 2002; Norman and Moerman, 2002; Praitis *et al.*, 2005; Lee *et al.*, 2010b; Wong *et al.*, 2015; Vuong-Brender *et al.*, 2017). However, much of our insight into the contribution of spectrin to contractile actomyosin networks has come from cell culture work (Tang *et al.*, 2003; Bournier *et al.*, 2006; Metral *et al.*, 2009; Collec *et al.*, 2011; Stankewich *et al.*, 2011), and experiments in live animals are lacking, with one notable exception in *Drosophila* (Wong *et al.*, 2015). Our work suggests that the *C. elegans* spermatheca may serve as a tractable model system for the elucidation of the role of spectrin in the organization and maintenance of contractile systems in vivo. We suggest that the spectrin cytoskeleton is part of a mechanism promoting reinforcement of actin bundles during contraction in the spermatheca.

MATERIALS AND METHODS

Caenorhabditis elegans strains and culture

All nematode strains were maintained on NGM (0.107 M NaCl, 0.25% wt/vol Peptone [Fisher Science Education], 1.7% wt/vol BD Bacto-Agar [Fisher Scientific], 0.5% Nyastatin [Sigma], 0.1 mM $CaCl_2$, 0.1 mM $MgSO_4$, 0.5% wt/vol cholesterol, 2.5 mM KPO_4) agar plates seeded with OP50 *Escherichia coli* at 23°C (Hope, 1999). Generation of nematode strains for this study was done by standard microinjection (Mello *et al.*, 1991). All constructs were injected at a concentration between 5 and 10 ng/µl with injection markers *rol-6* and *ttx3p*::RFP injected at 40 ng/µl and myo-2::GFP injected at 5 ng/µl. Carrier DNA, sheared, denatured salmon sperm DNA (Clontech, Mountain View, CA), was added to bring the final DNA concentration to 100 ng/µl for each injection mix. Extrachromosomal arrays were integrated by UV irradiation essentially as described in Mariol *et al.* (2013). Nematode observations and manipulations were performed at 23°C unless otherwise noted. *Caenorhabditis elegans* strains carrying alleles *plc-1(rx1), unc-70(n493),* and *unc-70(e542)* were obtained from the Caenorhabditis Genetics Center. The strain EG4492 carries the null allele *unc-70(s1502)* and transgene *oxIs95* rescuing *unc-70* expression in the hypodermis under the *pdi-2* promoter was generously provided by the Jorgensen lab (University of Utah, Salt Lake City, UT,) and has been described previously (Hammarlund *et al.*, 2007). Line AZ110 expressing SMA-1::GFP was a kind gift from the Praitis lab (Grinnell College, Grinnell, IA) and has been described previously (Praitis *et al.*, 2001, 2005). Strain COP1720 expressing *spc-1::degron::mKate2* at the endogenous locus was generated by NemaMatrix (Eugene, OR,), characterized by genomic sequencing, and generously provided by the Zaidel-Bar lab (Tel-Aviv University, Tel-Aviv, Israel). Line COP1720 was backcrossed three times to generate strain UN1823. Transgene *qyIs198[inft-1p::moeABD::mCherry, unc-119(+)]* was obtained from strain NK1069, a kind gift from the Sherwood lab (Duke University, Durham, NC). For a list of strains used in this study, please see Supplemental Table 1.

Expression constructs

Construct *fln-1p::GFP::act-1* was generated by restriction digest cloning to insert the *fln-1* promoter into pPRRF207 (*him-4p::GFP::act-1*) provided by the Roy lab (University of Toronto, Toronto, Canada) and has been described previously (Dixon and Roy, 2005). The *fln-1p::GFP::UtrCH* construct was generated by amplifying the mammalian utrophin calponin homology domain (UtrCH; actin-binding domain) from GFP-UtrCH (addgene #26737) and using restriction digest cloning to insert UtrCH into a plasmid backbone with *fln-1p::GFP.* The use of GFP-UtrCH to label F-actin has been described previously (Burkel *et al.*, 2007). Construct *fln-1p::ajm-1::GFP* was generated by amplifying the first nine exons of *ajm-1* from *C. elegans* gDNA and using restriction cloning to insert the *ajm-1* coding sequence upstream of GFP. The GFP was then replaced with tagRFP to generate *fln-1p::ajm-1::tagRFP.* The UNC-70 translational reporter was generated by using round horn PCR to remove mVenus from plasmid MG319 (*unc-70::TSMod;* addgene #73367) described previously (Krieg *et al.*, 2014). NEBuilder (NEB, Ipswich, MA) was used to clone the *unc-70::mTFP* fusion downstream of ~2 kb of the *unc-70* promoter region, amplified from *C. elegans* gDNA, in frame with the third exon of isoform A that is shared by all splice isoforms. The *fln-1p::TIR1::F2A::mCherry::h2b* construct was generated using NEBuilder (NEB, Ipswich, MA). The TIR1 coding sequence was amplified from the plasmid pLZ31 (addgene #71720) described previously (Zhang *et al.*, 2015). The histone coding sequence (*h2b*) was amplified from the plasmid pJH4.52 (addgene #26946) described previously (Gallo *et al.*, 2008) and inserted in frame with an mCherry fluorescent marker separated from the TIR1 coding sequence by the 22-amino-acid F2A peptide sequence, which was ordered as an oligo (Genewiz, South Plainfield, NJ). Use of the F2A peptide to coexpress separate proteins from the same mRNA has been previously validated in *C. elegans* (Ahier and Jarriault, 2014). Cloning details and plasmid sequences are available on request.

RNA interference

The RNAi feeding protocol was performed essentially as described in Timmons *et al.* (2001). To prepare seeded NGM–isopropylthio-β-galactoside (IPTG) plates, HT115(DE3) bacteria transformed with the double-stranded RNA (dsRNA) construct of interest were grown overnight at 37°C in Luria broth (LB) supplemented with 40 µg/ml ampicillin. The following day, 150 µl of the culture was seeded on NGM-IPTG agar (NGM supplemented with 25 µg/ml carbenicillin and 1 mM IPTG) and incubated at room temperature for 24–72 h to induce dsRNA expression. Age synchronized animals, prepared as described below, were then transferred to these plates.

Partially synchronized populations were obtained by alkaline lysis procedure ("egg prep"), and tightly synchronized populations were obtained by larval stage 1 (L1) arrest. For egg prep, starved dauer nematodes were allowed to recover for 48 h on NGM plates newly seeded with OP50. This produces young gravid adults for egg collection. Eggs were released using an alkaline hypochlorite solution as described in Hope (1999) and washed three times with filter sterilized M9 buffer (22 mM KH_2PO_4, 42 mM $NaHPO_4$, 86 mM NaCl, and 1 mM $MgSO_4$) (Hope, 1999). Clean eggs were then transferred to seeded NGM-IPTG plates. The L1 arrest protocol was adapted from Hope (1999). For L1 arrest, the same alkaline lysis procedure was performed, except clean eggs were transferred onto NGM without bacteria. Eggs were allowed to hatch and develop until L1 at 16°C overnight before being transferred to seeded NGM-IPTG plates. Populations produced by egg prep are ~10 h behind L1 arrest populations developmentally. All RNAi experiments were performed at 23°C. Strains utilized in each RNAi experiment are indicated.

RNAi constructs were obtained from the *ORFeome-RNAi v1.1 library* or were constructed by PCR amplification of wild-type cDNA and cloned into pPD129.36 (Fire Vector Kit). Empty pPD129.36 vector was used as a negative control in RNAi experiments. All primer sequences and cloning details are available on request.

RNAi screen of actin-binding and regulatory proteins

The Ontology Browser on WormBase (wormbase.org) was used to identify genes that encode proteins with conserved actin-binding domains that recognize either filamentous actin (F-actin) or monomeric, globular (G-actin) as well as proteins with conserved domains involved in actin filament bundling and organization (WormBase Gene Ontology IDs: GO:0051015, GO:0003785, GO:0003779, GO:0051017, and GO:0007015). In total, 103 genes were identified using this approach, and 102 genes, excluding *vab-10*, were scored for spermathecal contractility defects. Knockdown of VAB-10, spectraplakin, resulted in disrupted gonad morphology that precluded scoring (Morrissey *et al.*, 2014). The feeding method was selected to administer dsRNA to allow for continuous dsRNA exposure during post–embryonic development to achieve efficient RNAi in adult animals. However, RNAi efficiencies can differ for specific genes depending on the dsRNA delivery method (Kamath *et al.*, 2001). Therefore, the results of this RNAi screen may differ for specific genes compared with previous screens (Green *et al.*, 2011). RNAi was performed as described above. Partially synchronized populations were obtained by egg prep. Animals were grown for 65 h at 23°C and scored as adults. At this time, animals fed control RNAi have undergone several ovulations and contain embryos within the uterus. Spermathecae in live animals were visualized on the dissection scope using a line that expresses GFP::ACT-1 under a spermatheca specific promoter. This line allows for easy visualization of the spermatheca to distinguish spermathecae undergoing ovulation that are occupied by an oocyte and appear distended, "occupied," from spermathecae between ovulations that contain only sperm and appear compact, "empty." Animals with occupied spermathecae but no embryos in the uterus were scored as, "occupied on first," and animals with empty spermathecae and no embryos in the uterus were scored as, "no entry." At least 100 animals were scored for each condition (Supplemental Table 1). To ensure the same animal was not counted more than once, animals were removed from the plate by suction with a vacuum line as they were counted. Genes that resulted in a two- to –fourfold increase in the percentage of animals with occupied spermathecae were classified as resulting in a mild contractility defect. Genes that resulted in a greater than fourfold increase were classified as resulting in a severe contractility defect. Genes that resulted in a "no entry" phenotype were classified as resulting in a mild entry defect if fewer than 50% of animals had the "no entry" phenotype and a severe entry defect if 50% or more did.

Quantification of spermathecal contractility in unlabeled animals

Synchronized populations obtained by egg prep, described above, were grown on NGM-IPTG plates with the indicated RNAi treatment and worms were scored ~65 h after egg prep. Worms were mounted on a 2% agarose in water pad and killed using 100 mM sodium azide. Scoring for occupancy of spermathecae was done using a 60× oil-immersion objective with a Nikon Eclipse 80i microscope.

Histochemistry

For detection of an EMO phenotype, partially synchronized populations were obtained by egg prep and grown at 23°C for 65 h. Note that animals carrying alleles of *unc-70* aged more slowly and were grown for 70 h. For quantification of F-actin organization, tightly synchronized populations were obtained by L1 arrest and grown at 23°C for 40 or 45 h for animals carrying the *unc-70* alleles. At this time point, N2 control animals have just begun to ovulate. F-actin staining was adapted from Ono *et al.* (2007). Briefly, animals were dissected using a 25-gauge hypodermic needle in phosphate-buffered saline (PBS), and dissected gonads were fixed in 1.85% formaldehyde in PBS for 25 min at room temperature. Following fixation, gonads were washed twice with PBS, permeabilized for 15 min in PBST (PBS + 0.1% Triton X-100), and then incubated with 0.4 U/ml Texas Red-X phalloidin in PBS (Invitrogen, Carlsbad, CA,) overnight at 4°C or 3 h at room temperature. For identification of the Emo phenotype, nuclear stain, DAPI (Sigma-Aldrich, St. Louis, MO), was included at 100 ng/ml. Labeled samples were washed twice with PBS and mounted on 2% agarose pads for observation.

Confocal microscopy

For ovulation movies and observations of live or fixed animals, partially synchronized populations were obtained by egg prep and animals were grown at 23°C for ~50 h, around the time of the first ovulation. Live animals were immobilized with 0.01% tetramisole and 0.1% tricaine in M9 buffer (Kirby *et al.*, 1990; Mccarter *et al.*, 1997) and mounted on 2% agarose pads or with 0.05 µm Polybead Microspheres (Polysciences, Warrington, PA) diluted 1:2 in water and mounted on 5% agarose pads, adapted from Wang and Audhya (2014). Whole animals were fixed by transferring to 1.85% formaldehyde in PBS for 20 min at room temperature. Animals were then rinsed once with PBST and three times with PBS before being mounted on 2% agarose pads. Confocal microscopy was performed on an LSM 710 confocal microscope (Zeiss) equipped with Zen software (Zeiss) using the Plan-Apochromat 63×/1.40 Oil DIC M27 objective. The 405-nm laser was used to excite DAPI, 488-nm laser was used for GFP, and 561-nm laser was used for mCherry, mKate2, and TexasRed. For movies, 40 z-slices were acquired at 14-s intervals. Illumination of the spermathecae from animals expressing actin labeled with GFP (GFP::ACT-1) with the 488-nm laser for ~5 min prior to oocyte entry frequently caused the valve to remain partially closed during ovulation, increasing oocyte dwell time. For movies of all lines, live animals were imaged for ~30 min total. For still images of live and fixed animals and tissue, z-slices were acquired at 0.38-µm intervals with each slice representing the average of two scans or four scans.

Auxin-induced decay

The auxin-induced decay (AID) procedure was adapted from Zhang *et al.* (2015). Auxin-containing plates were made by adding 400 mM stock of 3-indoleacetic acid (IAA; Sigma-Aldrich I-2886, CAS Number 87-51-4) dissolved in 200-proof ethanol (Fisher) to cooled NGM media just before pouring plates. For control plates, 1% vol/vol 200 proof ethanol (Fisher) was added in place of the IAA stock. Plates were seeded with concentrated OP50 as described previously (Zhang *et al.*, 2015). The expression level of TIR1 was optimized to minimize background degradation of degron tagged SPC-1 at the endogenous locus in the absence of IAA. Animals expressing the TIR1 construct injected at 20 ng/µl had diminished SPC-1::degron::mKate2 fluorescence and disrupted spermathecal actin (visualized using GFP::UtrCH) on control plates and were excluded from analysis while animals expressing TIR1 injected at 10 ng/µl appeared WT in the absence of IAA. In preliminary experiments, young adult animals were exposed to IAA at concentrations of 0.25, 0.5, 1, and 4 mM for 5 h. Only the 1 and 4 mM IAA-treated animals showed complete reduction in mKate2 fluorescence with the 4 mM

condition producing the most consistent results. Young adults were then exposed to 4 mM IAA and monitored at 1 h intervals. By 4 h SPC-1::degron::mKate2 fluorescence was below detectable levels in the spermatheca. These animals were transferred to control plates and observed 24 h later for SPC-1::degron::mKate2 fluorescence recovery. However, fluorescence levels remained below detectable levels after 24 h.

To determine the role of SPC-1 postdevelopment, animals expressing *spc-1::degron::mKate2*, *Fln-1p::GFP::UtrCH*, and *Fln-1p::TIR1::F2A::mCherry::H2B* were "egg prepped" onto control plates and grown at 23°C for ~58 h. At this time, some animals are just before the first ovulation and many have already begun to ovulate. Approximately 100 animals just before the first ovulation and 100 animals that had undergone approximately two to five ovulations were segregated onto plates containing 4 mM IAA and returned to 23°C for 7 h along with the animals that remained on the control plate. Animals were also directly "egg prepped" onto 4 mM IAA and grown at 23°C for 65 h. The *fln-1* promoter driving *TIR1::F2A::mCherry::H2B* turns on during early L4 and remains on throughout adulthood (Kovacevic and Cram, 2010) therefore animals "egg prepped" onto IAA plates begin degrading degron tagged SPC-1 during L4 when the TIR1 construct is expressed. Animals from all conditions were dissected to excise gonads and fixed as described in the histochemistry section without incubation with phalloidin or DAPI and mounted on 2% agarose pads for observation.

Image analysis

ImageJ software was used for all image analysis. For consistency, all analysis was performed on cells of the main spermathecal bag unless otherwise indicated. For quantification of actin bundle fluorescence intensity in fixed samples, measurements were taken from a single confocal z-slice. A 20-pixel-wide line was drawn across each cell. BAR script Find Peaks was used to identify central and peripheral actin fluorescence peaks. For normalization, the central actin peak intensity measurements of an individual cell were divided by the largest peripheral actin fluorescence measurement of that cell. For analysis of actin fluorescence intensity in ovulation movies, measurements were taken at 70-s intervals (Five frames) from maximum intensity projections of confocal ovulation movies. As for fixed samples, a 20-pixel-wide line was drawn across each cell. Noise in images acquired using fast acquisition settings to capture actin dynamics in live animals precluded reliable identification of central actin peaks using the BAR script. Actin peaks at the cell periphery were identified using the BAR script, or manually when not possible, and measurement of peripheral actin peak intensity was calculated by taking the average of 10 pixels to the left and right of the identified peripheral peak. Central actin fluorescence was calculated by taking the average fluoresces across the entire 20-pixel-wide line, excluding pixels included in peripheral actin measurement. Normalized measurements were calculated by dividing the central actin measurement of a single cell by the largest peripheral actin measurement for that same cell. OrientationJ (Rezakhaniha *et al.*, 2012), configured using a Gaussian fit with a pixel size of 2, was used to measure the orientation distribution of actin bundles in individual cells and to generate color-coded images where color indicates orientation, hue indicates coherency, and brightness is the brightness of the original image.

Statistical analysis

All statistical analysis was performed with GraphPad Prism software. To compare two unpaired groups, the unpaired *t* test was used to determine whether the difference between the means of two data sets was significant when data had a normal distribution and Welch's correction was included if the different treatments were expected to have different standard deviations. To compare three or more unmatched groups, ordinary one-way analysis of variance was performed with either a Dunnett's multiple comparison or Tukey's multiple comparison test as necessary. The Mann–Whitney test was used when data did not have a normal distribution. All trapping data were analyzed using the Fisher's exact test. In all cases, the statistical test used and resulting *p* values, indicated by symbols ns ($p > 0.05$), *($p \leq 0.05$), **($p \leq 0.01$), ***($p \leq 0.001$), ****($p \leq 0.0001$), are noted in each figure caption.

ACKNOWLEDGMENTS

We thank Ronen Zaidel-Bar for critical discussions that shaped the manuscript. We also thank Ronen-Zaidel Bar, Vida Praitis, Erik Jorgensen, and David R. Sherwood for providing nematode strains used in this study. Additional strains used in this study were provided by the *Caenorhabditis* Genetics Center, which is funded by the National Center for Research Resources, National Institutes of Health. This work was supported by a grant from the National Institutes of Health/National Institute of General Medical Sciences (GM110268) to E.J.C.

REFERENCES

Ahier A, Jarriault S (2014). Simultaneous expression of multiple proteins under a single promoter in Caenorhabditis elegans via a versatile 2A-based toolkit. Genetics 196, 605–613.

Ammit AJ, Armour CL, Black JL (2000). Smooth-muscle myosin light-chain kinase content is increased in human sensitized airways. Am J Respir Crit Care Med 161, 257–263.

Bennett V, Baines AJ (2001). Spectrin and ankyrin-based pathways: metazoan inventions for integrating cells into tissues. Physiol Rev 81, 1353–1392.

Benz PM, Blume C, Moebius J, Oschatz C, Schuh K, Sickmann A, Walter U, Feller SM, Renné T (2008). Cytoskeleton assembly at endothelial cell-cell contacts is regulated by αII-spectrin-VASP complexes. J Cell Biol 180, 205–219.

Bournier O, Kroviarski Y, Rotter B, Nicolas G, Lecomte MC, Dhermy D (2006). Spectrin interacts with EVL (Enabled/vasodilator-stimulated phosphoprotein-like protein), a protein involved in actin polymerization. Biol Cell 98, 279–293.

Buechner M, Hall DH, Bhatt H, Hedgecock EM (1999). Cystic canal mutants in Caenorhabditis elegans are defective in the apical membrane domain of the renal (excretory) cell. Dev Biol 214, 227–241.

Burkel BM, Dassow Gon, Bement WM (2007). Versatile fluorescent probes for actin filaments based on the actin-binding domain of utrophin. Cell Motil Cytoskeleton 64, 822–832.

Burridge K, Wittchen ES (2013). The tension mounts : Stress fibers as force-generating mechanotransducers. J Cell Biol 200, 9–19.

Cecchetelli AD, Hugunin J, Tannoury H, Cram EJ (2016). CACN-1 is required in the Caenorhabditis elegans somatic gonad for proper oocyte development. Dev Biol 414, 58–71.

Chanet S, Miller CJ, Vaishnav ED, Ermentrout B, Davidson LA, Martin AC (2017). Actomyosin meshwork mechanosensing enables tissue shape to orient cell force. Nat Commun 8, 1–13.

Cianci CD, Zhang Z, Pradhan D, Morrow JS (1999). Brain and muscle express a unique alternative transcript of αII spectrin. Biochemistry 38, 15721–15730.

Collec E, Lecomte M-C, El Nemer W, Colin Y, Le Van Kim C (2011). Novel role for the Lu/BCAM–spectrin interaction in actin cytoskeleton reorganization. Biochem J 436, 699–708.

Cram EJ, Clark SG, Schwarzbauer JE (2003). Talin loss-of-function uncovers roles in cell contractility and migration in C. elegans. J Cell Sci 116, 3871–3878.

de Cuevas M, Lee JK, Spradling AC (1996). alpha-spectrin is required for germline cell division and differentiation in the Drosophila ovary. Development 122, 3959–3968.

Demarco RS, Lundquist EA (2010). RACK-1 acts with Rac GTpase signaling and UNC-115/abLIM in Caenorhabditis elegans axon pathfinding and cell migration. PLos Genet 6, e1001215.

Deng H, Xia D, Fang B, Zhang H (2007). The flightless I homolog, fli-1, regulates anterior/posterior polarity, asymmetric cell division and ovulation during Caenorhabditis elegans development. Genetics 177, 847–860.
Devarajan P, Stabach PR, De Matteis MA, Morrow JS (1997). Na,K-ATPase transport from endoplasmic reticulum to Golgi requires the Golgi spectrin-ankyrin G119 skeleton in Madin Darby canine kidney cells. Proc Natl Acad Sci USA 94, 10711–10716.
Dixon SJ, Roy PJ (2005). Muscle arm development in Caenorhabditis elegans. Development 132, 3079–3092.
Dominguez R (2004). Actin-binding proteins—a unifying hypothesis. Trends Biochem Sci 29, 572–578.
Dosemeci A, Reese TS (1995). Effect of calpain on the composition and structure of postsynaptic densities. Synapse 20, 91–97.
Dubreuil RR, Frankel J, Wang P, Howrylak J, Kappil M, Grushko TA (1998). Mutations of α spectrin and labial block cuprophilic cell differentiation and acid secretion in the middle midgut of Drosophila larvae. Dev Biol 194, 1–11.
Dubreuil RR, Maddux PB, Grushko Ta, MacVicar GR (1997). Segregation of two spectrin isoforms: polarized membrane-binding sites direct polarized membrane skeleton assembly. Mol Biol Cell 8, 1933–1942.
Dubreuil RR, Wang P, Dahl S, Lee J, Goldstein LSB (2000). Drosophila β spectrin functions independently of α spectrin to polarize the Na,K ATPase in epithelial cells. J Cell Biol 149, 647–656.
Faddis BT, Hasbani MJ, Goldberg MP (1997). Calpain activation contributes to dendritic remodeling after brief excitotoxic injury in vitro. J Neurosci 17, 951–959.
Ferrier A, Charron A, Sadozai Y, Switaj L, Szutenbach A, Smith PA (2011). Multiple phenotypes resulting from a mutagenesis screen for pharynx muscle mutations in Caenorhabditis elegans. PLoS One 6, e26594.
Flores C, Ma S-F, Maresso K, Ober C, Garcia JGN (2007). A variant of the myosin light chain kinase gene is associated with severe asthma in African Americans. Genet Epidemiol 31, 296–305.
Gallo CM, Munro E, Rasoloson D, Merritt C, Seydoux G (2008). Processing bodies and germ granules are distinct RNA granules that interact in C. elegans embryos. Dev Biol 323, 76–87.
Gao L, Grant AV, Rafaels N, Stockton-Porter M, Watkins T, Gao P, Chi P, Muñoz M, Watson H, Dunston G, *et al.* (2007). Polymorphisms in the myosin light chain kinase gene that confer risk of severe sepsis are associated with a lower risk of asthma. J Allergy Clin Immunol 119, 1111–1118.
Gibert MA, Starck J, Beguet B (1984). Role of the gonad cytoplasmic core during oogenesis of the nematode Caenorhabditis elegans. Biol Cell 50, 77–85.
Green RA, Kao HL, Audhya A, Arur S, Mayers JR, Fridolfsson HN, Schulman M, Schloissnig S, Niessen S, Laband K, *et al.* (2011). A high-resolution C. elegans essential gene network based on phenotypic profiling of a complex tissue. Cell 145, 470–482.
Greenquist AC, Shohet SB, Bernstein SE (1978). Marked reduction of spectrinin hereditary spherocytosis in the common house mouse. Blood 51, 1149 LP-1155.
Hammarlund M, Davis WS, Jorgensen EM (2000). Mutations in beta-spectrin disrupt axon outgrowth and sarcomere structure. J Cell Biol 149, 931–942.
Hammarlund M, Jorgensen EM, Bastiani MJ (2007). Axons break in animals lacking β-spectrin. J Cell Biol 176, 269–275.
Haviv L, Gillo D, Backouche F, Bernheim-Groswasser A (2008). A cytoskeletal demolition worker: myosin II acts as an actin depolymerization agent. J Mol Biol 375, 325–330.
Hegsted A, Wright FA, Votra S, Pruyne D (2016). INF2- and FHOD-related formins promote ovulation in the somatic gonad of C. elegans. Cytoskeleton 73, 712–728.
Higashi T, Arnold TR, Stephenson RE, Dinshaw KM, Miller AL (2016). Maintenance of the epithelial barrier and remodeling of cell-cell junctions during cytokinesis. Curr Biol 26, 1829–1842.
Hirsh D, Oppenheim D, Klass M (1976). Development of the reproductive system of Caenorhabditis elegans. Dev Biol 49, 200–219.
Holleran EA, Ligon LA, Tokito M, Stankewich MC, Morrow JS, Holzbaur ELF (2001). Beta III spectrin binds to the Arp1 subunit of dynactin. J Biol Chem 276, 36598–36605.
Holleran EA, Tokito MK, Karki S, Holzbaur ELF (1996). Centractin (ARP1) associates with spectrin revealing a potential mechanism to link dynactin to intracellular organelles. J Cell Biol 135, 1815–1829.
Hope IA (1999). C. elegans—A Practical Approach, Oxford, UK: Oxford University Press.
Hubbard EJ, Greenstein D (2000). The Caenorhabditis elegans gonad: a test tube for cell and developmental biology. Dev Dyn 218, 2–22.
Hulsmeier J, Pielage J, Rickert C, Technau GM, Klambt C, Stork T (2007). Distinct functions of α-Spectrin and β-Spectrin during axonal pathfinding. Development 134, 713–722.
Humphries JD, Wang P, Streuli C, Geiger B, Humphries MJ, Ballestrem C (2007). Vinculin controls focal adhesion formation by direct interactions with talin and actin. J Cell Biol 179, 1043–1057.
Iwasaki K, McCarter J, Francis R, Schedl T (1996). emo-1, a Caenorhabditis elegans Sec61p gamma homologue, is required for oocyte development and ovulation. J Cell Biol 134, 699–714.
Johansson M, Rocha N, Zwart W, Jordens I, Janssen L, Kuijl C, Olkkonen VM, Neefjes J (2007). Activation of endosomal dynein motors by stepwise assembly of Rab7-RILP-p150Glued, ORP1L, and the receptor βIII spectrin. J Cell Biol 176, 459–471.
Johnsen RC, Baillie DL (1991). Genetic analysis of a major segment [LGV(left)] of the genome of Caenorhabditis elegans. Genetics 129, 735 LP-752.
Kamath RS, Martinez-Campos M, Zipperlen P, Fraser AG, Ahringer J (2001). Effectiveness of specific RNA-mediated interference through ingested double-stranded RNA in Caenorhabditis elegans. Genome Biol 2, RESEARCH0002.
Kaunas R, Nguyen P, Usami S, Chien S (2005). Cooperative effects of Rho and mechanical stretch on stress fiber organization. Proc Natl Acad Sci USA 102, 15895–15900.
Kelley CA, Wirshing ACE, Zaidel-Bar R, Cram EJ (2018). The myosin light-chain kinase, MLCK-1, relocalizes during *Caenorhabditis elegans* ovulation to promote actomyosin bundle assembly and drive contraction. Mol Biol Cell 29, 1975–1991.
Kim JH, Kwon SJ, Stankewich MC, Huh GY, Glantz SB, Morrow JS (2016). Reactive protoplasmic and fibrous astrocytes contain high levels of calpain-cleaved alpha 2 spectrin. Exp Mol Pathol 100, 1–7.
Kirby C, Kusch M, Kemphues K (1990). Mutations in the par genes of Caenorhabditis elegans affect cytoplasmic reorganization during the first cell cycle. Dev Biol 142, 203–215.
Kizhatil K, Davis JQ, Davis L, Hoffman J, Hogan BLM, Bennett V (2007). Ankyrin-G is a molecular partner of E-cadherin in epithelial cells and early embryos. J Biol Chem 282, 26552–26561.
Kovacevic I, Cram EJ (2010). FLN-1/Filamin is required for maintenance of actin and exit of fertilized oocytes from the spermatheca in C. elegans. Dev Biol 347, 247–257.
Kovacevic I, Orozco JM, Cram EJ (2013). Filamin and phospholipase C-ε are required for calcium signaling in the caenorhabditis elegans spermatheca. PLoS Genet 9, e1003510.
Kranewitter WJ, Ylanne J, Gimona M (2001). UNC-87 Is an actin-bundling protein. J Biol Chem 276, 6306–6312.
Krieg M, Dunn AR, Goodman MB (2014). Mechanical control of the sense of touch by β-spectrin. Nat Cell Biol 16, 224–233.
Lavoie TL, Dowell ML, Lakser OJ, Gerthoffer WT, Fredberg JJ, Seow CY, Mitchell RW, Solway J (2009). Disrupting actin-myosin-actin connectivity in airway smooth muscle as a treatment for asthma? Proc Am Thorac Soc 6, 295–300.
Lee A, Morrow JS, Fowler VM (2001). Caspase remodeling of the spectrin membrane skeleton during lens development and aging. J Biol Chem 276, 20735–20742.
Lee C, Haase C, Deguchi S, Kaunas R (2010a). Cyclic stretch-induced stress fiber dynamics—dependence on strain rate, Rho-kinase and MLCK. Biochem Biophys Res Commun 401, 344–349.
Lee H-G, Zarnescu DC, MacIver B, Thomas GH (2010b). The cell adhesion molecule Roughest depends on Heavy-spectrin during eye morphogenesis in Drosophila. J Cell Sci 123, 277–285.
Leerberg JM, Gomez GA, Verma S, Moussa EJ, Wu SK, Priya R, Hoffman BD, Grashoff C, Schwartz MA, Yap AS (2014). Tension-sensitive actin assembly supports contractility at the epithelial zonula adherens. Curr Biol 24, 1689–1699.
Leguillette R, Laviolette M, Bergeron C, Zitouni N, Kogut P, Solway J, Kachmar L, Hamid Q, Lauzon AM (2009). Myosin, transgelin, and myosin light chain kinase expression and function in asthma. Am J Respir Crit Care Med 179, 194–204.
Lencesova L, O'Neill A, Resneck WG, Bloch RJ, Blaustein MP (2004). Plasma membrane-cytoskeleton-endoplasmic reticulum complexes in neurons and astrocytes. J Biol Chem 279, 2885–2893.
Lenz M, Gardel ML, Dinner AR (2012). Requirements for contractility in disordered cytoskeletal bundles. New J Phys 14, 033037.
Li D, Harper SL, Tang HY, Maksimova Y, Gallagher PG, Speicher DW (2010). A comprehensive model of the spectrin divalent tetramer binding region deduced using homology modeling and chemical cross-linking of a mini-spectrin. J Biol Chem 285, 29535–29545.

Li D, Tang HY, Speicher DW (2008). A structural model of the erythrocyte spectrin heterodimer initiation site determined using homology modeling and chemical cross-linking. J Biol Chem 283, 1553–1562.
Lim JA, Baek HJ, Jang MS, Choi EK, Lee YM, Lee SJ, Lim SC, Kim JY, Kim TH, Kim HS, *et al.* (2014). Loss of β2-spectrin prevents cardiomyocyte differentiation and heart development. Cardiovasc Res 101, 39–47.
Lundquist EA, Herman RK, Shaw JE, Bargmann CI (1998). UNC-115, a conserved protein with predicted LIM and actin-binding domains, mediates axon guidance in C. elegans. Neuron 21, 385–392.
Machnicka B, Czogalla A, Hryniewicz-Jankowska A, Bogusławska DM, Grochowalska R, Heger E, Sikorski AF (2014). Spectrins: a structural platform for stabilization and activation of membrane channels, receptors and transporters. Biochim Biophys Acta 1838, 620–634.
Mariol M, Walter L, Bellemin S, Gieseler K (2013). A rapid protocol for integrating extrachromosomal arrays with high transmission rate into the C. elegans genome. J Vis Exp 82, e50773.
Mccarter J, Bartlett B, Dang T, Schedl T (1999). On the control of oocyte meiotic maturation and ovulation in caenorhabditis elegans. Dev Biol 205, 111–128.
Mccarter J, Bartlett B, Thanh D, Schedl T (1997). Soma–germ cell interactions in caenorhabditis elegans: multiple events of hermaphrodite germline development require the somatic sheath and spermathecal lineages. Dev Biol 143, 121–143.
McKeown C, Praitis V, Austin J (1998). sma-1 encodes a betaH-spectrin homolog required for Caenorhabditis elegans morphogenesis. Development 125, 2087–2098.
McMahon LW, Walsh CE, Lambert MW (1999). Human α spectrin II and the Fanconi anemia proteins FANCA and FANCC interact to form a nuclear complex. J Biol Chem 274, 32904–32908.
Medeiros NA, Burnette DT, Forscher P (2006). Myosin II functions in actin-bundle turnover in neuronal growth cones. Nat Cell Biol 8, 215–226.
Médina E, Williams J, Klipfell E, Zarnescu D, Thomas G, Le Bivic A (2002). Crumbs interacts with moesin and βHeavy-spectrin in the apical membrane skeleton of Drosophila. J Cell Biol 158, 941–951.
Mello CC, Kramer JM, Stinchcomb D, Ambros V (1991). Efficient gene transfer in C.elegans: extrachromosoal maintenance and integration of transforming sequences. EMBO 10, 3959–3970.
Metral S, Machnicka B, Bigot S, Colin Y, Dhermy D, Lecomte MC (2009). αII-spectrin is critical for cell adhesion and cell cycle. J Biol Chem 284, 2409–2418.
Molloy JE, Burns JE, Kendrick-Jones J, Tregear RT, White DC (1995). Movement and force produced by a single myosin head. Nature 378, 209–212.
Moon RT, McMahon AP (1990). Generation of diversity in nonerythroid spectrins: Multiple polypeptides are predicted by sequence analysis of cDNAs encompassing the coding region of human nonerythroid alpha-spectrin. J Biol Chem 265, 4427–4433.
Moorthy S, Chen L, Bennett V (2000). Caenorhabditis elegans β-G spectrin is dispensable for establishment of epithelial polarity, but essential for muscular and neuronal function. J Cell Biol 149, 915–930.
Morrissey MA, Keeley DP, Hagedorn EJ, McClatchey STH, Chi Q, Hall DH, Sherwood DR (2014). B-LINK: A hemicentin, plakin, and integrin-dependent adhesion system that links tissues by connecting adjacent basement membranes. Dev Cell 31, 319–331.
Muresan V, Stankewich MC, Steffen W, Morrow JS, Holzbaur ELF, Schnapp BJ (2001). Dynactin-dependent, dynein-driven vesicle transport in the absence of membrane proteins: A role for spectrin and acidic phospholipids. Mol Cell 7, 173–183.
Myers CD, Goh PY, Allen TS, Bucher EA, Bogaert T (1996). Developmental genetic analysis of troponin T mutations in striated and nonstriated muscle cells of Caenorhabditis elegans. J Cell Biol 132, 1061 LP-1077.
Nelson WJ, Shore EM, Wang AZ, Hammerton RW (1990). Identification of a membrane-cytoskeleton complex containing the cell adhesion molecule uvomorulin (E-Cadherin), ankyrin, and fodrin in Madin-Darby canine kidney epithelial cells. J Cell Biol 110, 349–357.
Nishimura K, Fukagawa T, Takisawa H, Kakimoto T, Kanemaki M (2009). An auxin-based degron system for the rapid depletion of proteins in nonplant cells. Nat Methods 6, 917–922.
Norman KR, Moerman DG (2002). α spectrin is essential for morphogenesis and body wall muscle formation in Caenorhabditis elegans. J Cell Biol 157, 665–677.
Obinata T, Ono K, Ono S (2010). Troponin I controls ovulatory contraction of non-striated actomyosin networks in the C. elegans somatic gonad. J Cell Sci 123, 1557–1566.
Ono K, Ono S (2004). Tropomyosin and troponin are required for ovarian contraction in the Caenorhabditis elegans reproductive system. Mol Biol Cell 15, 2782–2793.
Ono K, Ono S (2014). Two actin-interacting protein 1 isoforms function redundantly in the somatic gonad and are essential for reproduction in Caenorhabditis elegans. Cytoskeleton 71, 36–45.
Ono K, Ono S (2016). Two distinct myosin II populations coordinate ovulatory contraction of the myoepithelial sheath in the Caenorhabditis elegans somatic gonad. Mol Biol Cell 27, 1131–1142.
Ono K, Parast M, Alberico C, Benian GM, Ono S (2003). Specific requirement for two ADF/cofilin isoforms in distinct actin-dependent processes in Caenorhabditis elegans. J Cell Sci 116, 2073–2085.
Ono K, Yamashiro S, Ono S (2008). Essential role of ADF/cofilin for assembly of contractile actin networks in the C. elegans somatic gonad. J Cell Sci 121, 2662–2670.
Ono K, Yu R, Ono S (2007). Structural components of the nonstriated contractile apparatuses in the Caenorhabditis elegans gonadal myoepithelial sheath and their essential roles for ovulation. Dev Dyn 236, 1093–1105.
Piepenhagen PA, Nelson WJ (1998). Biogenesis of polarized epithelial cells during kidney development in situ: roles of E-cadherin-mediated cell-cell adhesion and membrane cytoskeleton organization. Mol Biol Cell 9, 3161–3177.
Ponceau A, Albigès-Rizo C, Colin-Aronovicz Y, Destaing O, Lecomte MC (2015). αII-spectrin regulates Invadosome stability and extracellular matrix degradation. PLoS One 10, 1–23.
Praitis V, Casey E, Collar D, Austin J (2001). Creation of low-copy integrated transgenic lines in Caenorhabditis elegans. Genetics 157, 1217–1226.
Praitis V, Ciccone E, Austin J (2005). SMA-1 spectrin has essential roles in epithelial cell sheet morphogenesis in C. elegans. Dev Biol 283, 157–170.
Dos Remedios CG, Chhabra D, Kekic M, Dedova IV, Tsubakihara M, Berry DA, Nosworthy NJ (2003). Actin binding proteins: regulation of cytoskeletal microfilaments. Physiol Rev 83, 433–473.
Rezakhaniha R, Agianniotis A, Schrauwen JTC, Griffa A, Sage D, Bouten CVC, van de Vosse FN, Unser M, Stergiopulos N (2012). Experimental investigation of collagen waviness and orientation in the arterial adventitia using confocal laser scanning microscopy. Biomech Model Mechanobiol 11, 461–473.
Ryabova LV, Virtanen I, Wartiovaara J, Vassetzky SG (1994). Contractile proteins and nonerythroid spectrin in oogenesis of Xenopus laevis. Mol Reprod Dev 37, 99–109.
Sears C, Kaunas R (2016). The many ways adherent cells respond to applied stretch. J Biomech 49, 1347–1354.
Shakir MA, Jiang K, Struckhoff EC, Demarco RS, Patel FB, Soto MC, Lundquist EA (2008). The Arp2/3 activators WAVE and WASP have distinct genetic interactions with Rac GTPases in Caenorhabditis elegans axon guidance. Genetics 179, 1957–1971.
Sisto M, Lorusso L, Ingravallo G, Tamma R, Nico B, Ribatti D, Ruggieri S, Lisi S (2018). Reduced myofilament component in primary Sjögren's syndrome salivary gland myoepithelial cells. J Mol Histol 49, 1–11.
Smith AS, Nowak RB, Zhou S, Giannetto M, Gokhin DS, Papoin J, Ghiran IC, Blanc L, Wan J, Fowler VM (2018). Myosin IIA interacts with the spectrin-actin membrane skeleton to control red blood cell membrane curvature and deformability. Proc Natl Acad Sci 115, 201718285.
Stankewich MC, Cianci CD, Stabach PR, Ji L, Nath A, Morrow JS (2011). Cell organization, growth, and neural and cardiac development require II-spectrin. J Cell Sci 124, 3956–3966.
Stankewich MC, Moeckel GW, Ji L, Ardito T, Morrow JS (2016). Isoforms of spectrin and ankyrin reflect the functional topography of the mouse kidney. PLoS One 11, 1–20.
Stankewich MC, Tse WT, Peters LL, Ch'ng Y, John KM, Stabach PR, Devarajan P, Morrow JS, Lux SE (1998). A widely expressed betaIII spectrin associated with Golgi and cytoplasmic vesicles. Proc Natl Acad Sci USA 95, 14158–14163.
Struckhoff EC, Lundquist EA (2003). The actin-binding protein UNC-115 is an effector of Rac signaling during axon pathfinding in C. elegans. Development 130, 693–704.
Svitkina T (2018). The actin cytoskeleton and actin-based motility. Cold Spring Harb Perspect Biol 10, a018267.
Tang Y, Katuir V, Dillner A, Mishra B, Deng C-X, Mishra L (2003). Disruption of transforming growth factor-beta signaling in ELF beta-spectrin-deficient mice. Science 299, 574–577.
Thomas GH, Kiehart DP (1994). Beta heavy-spectrin has a restricted tissue and subcellular distribution during Drosophila embryogenesis. Development 120, 2039–2050.

Thomas GH, Williams JA (1999). Dynamic rearrangement of the spectrin membrane skeleton during the generation of epithelial polarity in Drosophila. J Cell Sci 112 (Pt 1), 2843–2852.
Thomas GH, Zarnescu DC, Juedes AE, Bales MA, Londergan A, Korte CC, Kiehart DP (1998). Drosophila betaHeavy-spectrin is essential for development and contributes to specific cell fates in the eye. Development 125, 2125–2134.
Timmons L, Court DL, Fire A (2001). Ingestion of bacterially expressed dsRNAs can produce specific and potent genetic interference in Caenorhabditis elegans. Gene 263, 103–112.
Tse WT, Lecomte MC, Costa FF, Garbarz M, Feo C, Boivin P, Dhermy D, Forget BG (1990). Point mutation in the beta-spectrin gene associated with alpha I/74 hereditary elliptocytosis. Implications for the mechanism of spectrin dimer self-association. J Clin Invest 86, 909–916.
Uehata M, Ishizaki T, Satoh H, Ono T, Kawahara T, Morishita T, Tamakawa H, Yamagami K, Inui J, Maekawa M, *et al*. (1997). Calcium sensitization of smooth muscle mediated by a Rho-associated protein kinase in hypertension. Nature 389, 990–994.
Vuong-Brender TTK, Ben Amar M, Pontabry J, Labouesse M (2017). The interplay of stiffness and force anisotropies drives embryo elongation. Elife 6, 1–49.
Wang L, Audhya A (2014). In vivo imaging of C. elegans endocytosis. Methods 68, 518–528.
Ward S, Carrel JS (1979). Fertilization and sperm competition in the nematode Caenorhabditis elegans. Dev Biol 73, 304–321.
Wirshing ACE, Cram EJ (2017). Myosin activity drives actomyosin bundle formation and organization in contractile cells of the Caenorhabditis elegans spermatheca. Mol Biol Cell 28, 1937–1949.
Wolke U, Jezuit EA, Priess JR (2007). Actin-dependent cytoplasmic streaming in C. elegans oogenesis. Development 134, 2227–2236.
Wong KKL, Li W, An Y, Duan Y, Li Z, Kang Y, Yan Y (2015). B-spectrin regulates the hippo signaling pathway and modulates the basal actin network. J Biol Chem 290, 6397–6407.
Wu XT, Sun LW, Yang X, Ding D, Han D, Fan YB (2017). The potential role of spectrin network in the mechanotransduction of MLO-Y4 osteocytes. Sci Rep 7, 1–12.
Yang Y, Lundquist EA (2005). The actin-binding protein UNC-115/abLIM controls formation of lamellipodia and filopodia and neuronal morphogenesis in Caenorhabditis elegans. Mol Cell Biol 25, 5158–5170.
Yonemura S, Wada Y, Watanabe T, Nagafuchi A, Shibata M (2010). α-Catenin as a tension transducer that induces adherens junction development. Nat Publ Gr 12, 533–542.
Yu J, Fischman DA, Steck TL (1973). Selective solubilization of proteins and phospholipids from red blood cell membranes by nonionic detergents. J Supramol Struct 1, 233–248.
Yu R, Ono S (2006). Dual roles of tropomyosin as an F-actin stabilizer and a regulator of muscle contraction in Caenorhabditis elegans body wall muscle. Cell Motil Cytoskeleton 63, 659–672.
Zaidel-Bar R, Zhenhuan G, Luxenburg C (2015). The contractome—a systems view of actomyosin contractility in non-muscle cells. J Cell Sci 128, 2209–2217.
Zarnescu DC, Thomas GH (1999). Apical spectrin is essential for epithelial morphogenesis but not apicobasal polarity in Drosophila. J Cell Biol 146, 1075–1086.
Zhang L, Ward JD, Cheng Z, Dernburg AF (2015). The auxin-inducible degradation (AID) system enables versatile conditional protein depletion in C. elegans. Development 142, 4374–4384.
Zhang R, Zhang C, Zhao Q, Li D (2013). Spectrin: structure, function and disease. Sci China Life Sci 56, 1076–1085.